UNIVERSITY OF CALIFORNIA SAN DIEGO

Interrogating acute changes in the surface expression landscape of irradiated glioma stem cells using phage display

A thesis submitted in partial satisfaction of the
requirements for the degree of Master of Science

in

Bioengineering

by

Aaron Yu

Committee in charge:

Professor Ester Kwon, Chair
Professor Christian Metallo
Professor Jeremy Rich
Professor Jin Zhang

2021

The Thesis of Aaron Yu is approved, and it is acceptable in quality and form for publication on microfilm and electronically.

University of California San Diego

2021

DEDICATION

For my parents and friends who always believed in and supported me.

TABLE OF CONTENTS

LIST OF FIGURES

LIST OF TABLES

ACKNOWLEDGEMENTS

Firstly, I would like to thank Dr. Kwon for her willingness to step in as the committee chair during Jeremy's transition period, and I would like to thank the rest of the committee members, Dr. Metallo and Dr. Zhang, for their patience, kindness, and suggestions during the writing process.

I am also grateful to all of my friends and colleagues for helping out with the writing process and with figuring out my own life and to my co-workers for being understanding and supportive.

Additionally, I want to thank all of my collaborators, especially Naj and Tom who were saving graces during this time, and without whom I would not have been able to reach a satisfying completion. Naj and Tom have been extremely supportive and were kind enough to accept me into their lab for a short period to get me to the finish line. Naj was also especially helpful in the writing process, and I am extremely grateful to her for acting as an in-person advisor.

I want to extend a special thanks to all of the members of the Rich Lab, especially those that were always helping me out and making work fun. Thank you to Shira, Ryan, DD, Esther, Derrick, Lian, and Bri for supporting me and being awesome. Shira, Lian, and DD gave me a lot of good experimental advice and were always there to help me out with experiments and planning, which I greatly appreciate. Bri deserves an even more special shoutout for not only being fun, but also starting this entire project, passing it down to me, and always being available to chat and help out with whatever scientific mess I found myself in.

Lastly, my sincerest thanks extend to my advisor, committee member, and PI—Dr. Jeremy Rich—for putting up with me for an entire two years and finally seeing me become a somewhat competent scientist. In hindsight, it was a big risk to start in the Rich Lab with minimal experience, but somehow we both managed to get through it and I would definitely say it was a positive experience. Thank you for all of the pressure, advice, and creative freedom which managed to mold me into a somewhat capable scientist, and I would have loved to continue more exciting projects with you if things remained in San Diego.

This Thesis is coauthored with Briana Prager. The thesis author was the primary author of this Thesis.

ABSTRACT OF THE THESIS

Interrogating acute changes in the surface expression landscape of irradiated glioma stem cells using phage display

by

Aaron Yu

Master of Science in Bioengineering

University of California San Diego, 2021

Professor Ester Kwon, Chair

Glioblastoma is the deadliest form of brain cancer, yet treatment remains largely palliative. Recurrence and resistance to conventional radiation therapies are largely due to subsets of radioresistant glioma stem cells (GSCs) which survive and can repropagate the tumor. Phage display is a well-established high-throughput screening technique which can identify high-affinity, surface-binding peptides against targets of interest. We used phage display to identify a single peptide sequence, YPHKWHEFKQRV, which was highly enriched in irradiated patient-derived GSC neurospheres compared to both non-tumor populations and unirradiated GSCs. Irradiation significantly increased surface binding of the target peptide in a number of different patient-derived GSC neurospheres in vitro and in vivo. This binding increase was abrogated by dissociation into

single-cell suspensions prior to peptide binding, suggesting a possible cell-cell adhesion-related peptide binding partner. We identified four candidate genes which preferentially bind the peptide, and we observed aberrant plasma membrane localization in both Ezrin (EZR) and Metadherin (MTDH) following irradiation. All four candidate genes were essential for GSC proliferation based on shRNA knockdowns, while only EZR knockdown significantly impaired unirradiated proliferation, post-irradiation proliferation, and survival to ionizing radiation. Together, these data suggest a possible radiation-induced translocation mechanism for EZR supporting radioresistance uniquely in GSCs. Additionally, the specificity of the phage display-identified for irradiated GSCs highlight the power of this technique and the potential for this and other tumor-targeting peptides in GBM immunotherapy.

Chapter 1

Introduction

Gliomas are the most common primary intrinsic brain tumors and originate from the glial cells of the brain or spinal cord. The World Health Organization (WHO) classifies gliomas into four grades: grades I and II low-grade gliomas, grade III anaplastic astrocytoma and oligodendroglioma, and grade IV glioblastoma (*1*, *2*). Despite many efforts to improve therapeutic outcomes for patients, low-grade gliomas invariably progress to higher-grade neoplasms (WHO grades III and IV) over time (*3*). Glioblastoma (GBM) is the most common of these primary malignant brain tumors, accounting for 82% of all malignant gliomas and with an annual incidence rate of 17,000 new cases diagnosed per year (*3*). Moreover, the most significant recent advancement in the field of GBM therapy has been the adoption of temozolomide (TMZ) as the standard-of-care chemotherapeutic agent (*4*), boasting a modest median survival increase of only 2.5 months in patients receiving concomitant radiotherapy (*5*). However, despite the standard-of-care maximal surgical resection followed by conjunctive radiotherapy and chemotherapy, GBM remains a universally lethal cancer with a median survival of just 15 months (*4*). GBM therapy faces many challenges typically caused by tumor resistance resulting from immune evasion, tumor invasiveness, and intratumoral cellular heterogeneity (*6*–*8*). These include immunosuppression via programmed death ligand-1 (PD-L1) (*8*, *9*), invasion mediated by epithelial-to-mesenchymal transitions (EMT) (*10*, *11*), and heterogeneous intratumoral subpopulations resulting from spontaneous mutations (*12*, *13*). In addition to intratumoral cellular heterogeneity, genetic and epigenetic differences among tumors from different patients suggest varying individual responses to therapy and make developing

effective treatments even more difficult. While epidermal growth factor receptor (EGFR), TP53 (p53), and isocitrate dehydrogenase (IDH) mutations are considered to be some of the most common genetic alterations in GBM (57%, 28%, and 12%, respectively), only EGFR mutations constitute the majority of all GBM cases annotated in The Cancer Genome Atlas Research Network (TCGA) (*14*, *15*). However, there has been disappointing clinical success of several EGFR inhibitors (*16*, *17*). The extreme diversity of GBM tumors and the challenges to conventional therapies implicate the need for more targeted approaches to treatment options.

1.1 Cancer Stem Cells in Glioblastoma

While it has been known that many solid tumors are a non-homogeneous mosaic of cell types, recent evidence have suggested the existence of subsets of cancer cells with stem-like properties within the heterogeneous tumor milieu (*18*, *19*). Similarly to stem cells of non-neoplastic tissues, these so-called cancer stem cells (CSCs) are able to self-renew and differentiate, in addition to sustaining tumorigenesis (**Fig. 1A**) (*20*). CSCs were first documented in acute myeloid leukemia (AML) (*21*) after observations that only a small subset of mouse myeloma cells could form clonal colonies in vitro (*22*). Ever since, CSCs have been described and characterized in a number of solid tumor types including those of the brain, breast, colon, pancreas, lung, and skin (*20*).

Recently, tumor initiating cells were first functionally identified in GBM (*23*, *24*), suggesting a role for CSCs in brain cancers. Importantly, functionally-defined glioma stem cells (GSCs) have been shown to drive GBM tumorigenesis and resistance to conventional therapies by mediating angiogenesis (*25*, *26*), self-renewal (*27*), tumor invasiveness (*7*, *28*), intratumoral diversity (*6*, *29*), and resistance to chemotherapy (*30*, *31*) and radiotherapy (*32*). Furthermore, there has been increasing evidence that targeting unique genetic (*14*), epigenetic (*33*, *34*), epitranscriptomic (*35*), metabolic (*36*, *37*), and microenvironmental (*38*, *39*) GSC dependencies can lead to pronounced therapeutic benefits (**Fig. 1B**).

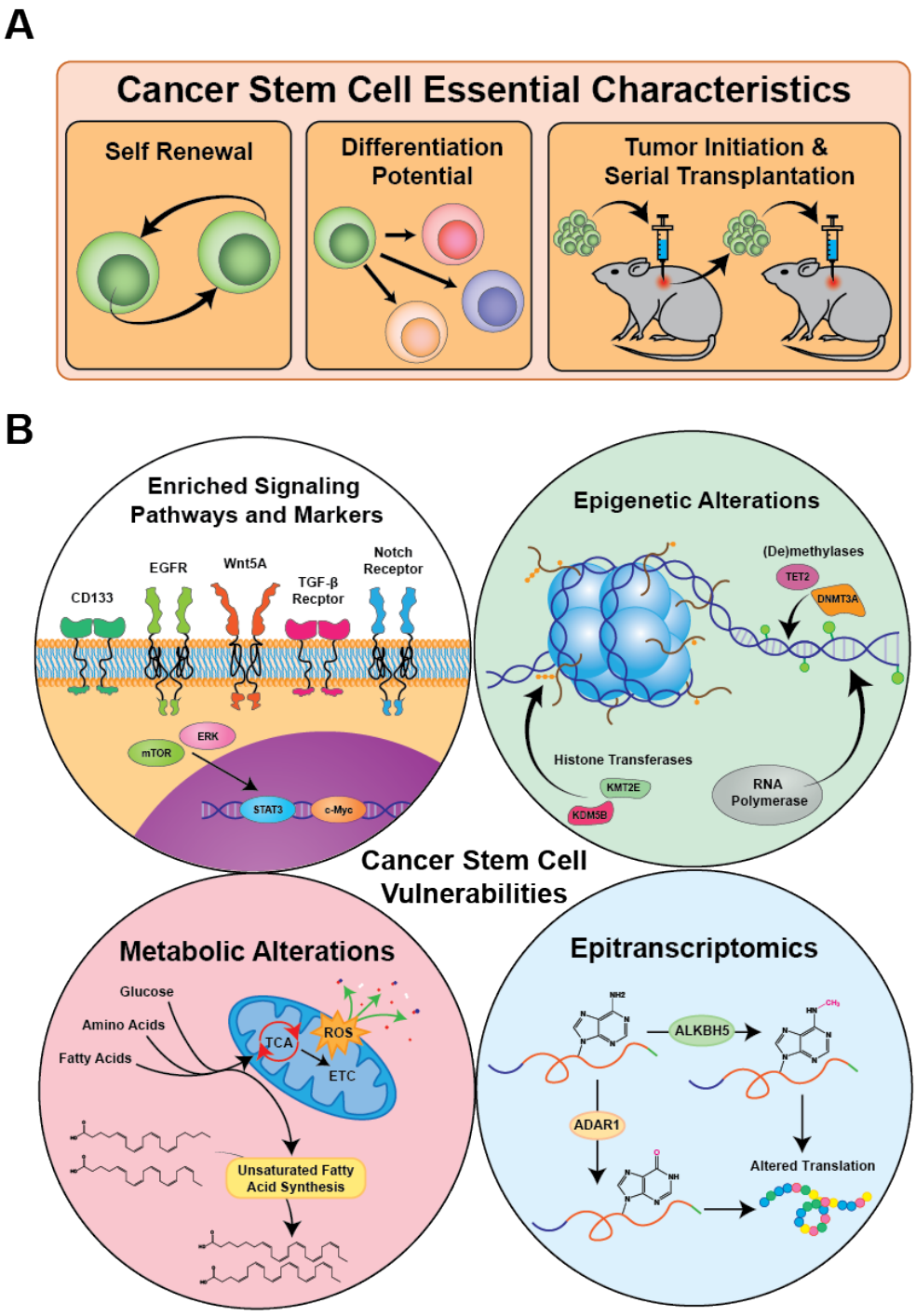

Figure 1. Functional characteristics and unique alterations in CSCs. (**A**) Diagram illustrating the characteristics required for functional classification CSCs. (**B**) Schematic depicting some of the unique signaling pathways and epigenetic, metabolic, and epitranscriptomic alterations dysregulated in CSCs.

An important limitation in CSC research is the lack of defining molecular markers. Several efforts have identified a number of surface markers that enrich for this rare and therapeutically critical subset of cells. These include CD44, CD133, CD24, and EpCAM in tumors of the breast, brain, colon, pancreas, and lung (*20*). Specifically in GSCs, several internal and surface molecular markers enrich for the stem cell phenotype, such as CD133, GPD1, and SOX2 (*24*, *40*, *41*). However, these markers are not definitive, and significant overlap with canonical non-tumor stem cell markers (e.g. SOX2, OLIG2, etc.) compounds the difficulty of identifying CSCs (*19*). Moreover, CSCs from different regions of the same tumor may present different surface proteomic landscapes (*6*, *41*), meaning that a single tumor may contain several populations of CSCs that are both molecularly and functionally distinct. Indeed, further studies to identify additional CSC enrichment markers will be critical for developing therapeutic strategies against this rare subset of tumor cells.

1.2 Radiation Therapy

The standard-of-care treatment for any patient diagnosed with GBM is maximal surgical resection followed by concomitant chemotherapy and radiotherapy (*4*). Because ionizing radiation therapy is such an integral therapeutic treatment, several studies have sought to identify the molecular dependencies and transient molecular changes induced by irradiation in a number of different cancer types. These include cell cycle arrest and DNA damage pathways associated with p53 and ataxia-telangiectasia mutated (ATM) proteins (*42*, *43*) and a transient increase in reactive oxygen species (ROS) generation (*44*), which has been shown to be a targetable tumor vulnerability (*45*). Similarly, in CSCs, several molecular changes associated with cell cycle arrest, DNA damage, and ROS generation pathways are dysregulated following radiation (*26*, *32*, *46–49*), suggesting possible synthetic vulnerabilities. It is well-documented that oncogenic pathways such as JAK-STAT (Janus kinase and signal transducer and activator of transcription proteins) and Notch can support radioresistance preferentially in CSCs and, thus, act as unique radiation-induced dependencies (*50*, *51*). Indeed, the observation that CSCs contribute significantly to overall tumor radioresistance (*52*) suggests an importance for studying the molecular changes that occur in acutely

radioresistant CSCs.

1.3 Phage Display

Bacteriophages—also known as phages—are viruses which infect and replicate in bacteria. They consist of coat proteins surrounding and protecting a cargo of genetic material which allows the phage to replicate. In particular, the M13 bacteriophage is a filamentous phage (inovirus) consisting of a number of major and minor coat proteins surrounding a cargo of single-stranded DNA which directly encodes for the translation of its coat proteins (*53*). It was discovered that foreign DNA fragments could be inserted into specific regions of the inovirus genome to create fusion coat proteins which were displayed on the virion's surface (*54*). These chimeric phages retained the ability to infect and replicate in bacteria, and they could be highly enriched over ordinary phage when panning against an antibody specific for the chimeric antigen. Expansion of this vector system to phages fused with libraries of antigens became known as phage display (*55*, *56*).

Recent advancements in phage display technology have improved its throughput and ability to screen binding affinities of large antigen libraries against samples of interest (*53*). Several studies have taken advantage of the surface-displayed nature of peptide-fused phage libraries to identify and target cell surface markers differentially present in a number of cancers (*57–59*). In the phage display workflow, a library of phages displaying a diverse set of peptides is panned against samples of interest. The unbound phages are washed away, while the bound phages are eluted and amplified in bacteria for sequencing (**Fig. 2**); these steps can be repeated iteratively to enrich for phages with high specificity for targets of interest (*59*, *60*). Some key advantages to this discovery platform include 1) the direct link between the phage's surface-displayed antigen and the phage's DNA (*54*, *60*); 2) the ability of phages to bind to the surface of live cells and be internalized, allowing for interrogation of the surface molecular landscape as well as internalization pathways (*61–64*); and 3) the ability to iteratively enrich—both positively and negatively (*59*)—for phages of interest from large libraries ($>10^9$). Previous works have validated the use of the phage display platform to

identify tumor-specific, surface-displayed binding motifs (*58*, *59*, *65–67*), demonstrating both the specificity and iterative process.

In this Thesis, I present the novel use of phage display to identify a peptide sequence specific for acutely irradiated GSCs and interrogate the mechanisms of its binding specificity. We identified a single fusion peptide with the highest phage enrichment in three irradiated patient-derived GSC lines. Indeed, irradiation induced increased cell surface binding of the peptide in several GSC lines *in vitro*, and the target peptide preferentially homed to irradiated GSC-derived tumors *in vivo*. We identified four intracellular candidate genes that may bind the peptide following irradiation and observed aberrant plasma membrane translocalization of two of the four after irradiation. To our knowledge, this is the first implication of these genes in aberrant plasma membrane translocation, and this mechanism may play a role in resistance to radiation therapies. Additionally, our work validates the use of phage display in identifying tumor-specific antigens, agnostic to the binding target's identity. Combined with the high-throughput screening advantage of phage display, these tumor-specific peptides have great potential as possible tumor-targeting moieties in immuno- and co-immunotherapies such as chimeric antigen receptor (CAR) T cell therapy.

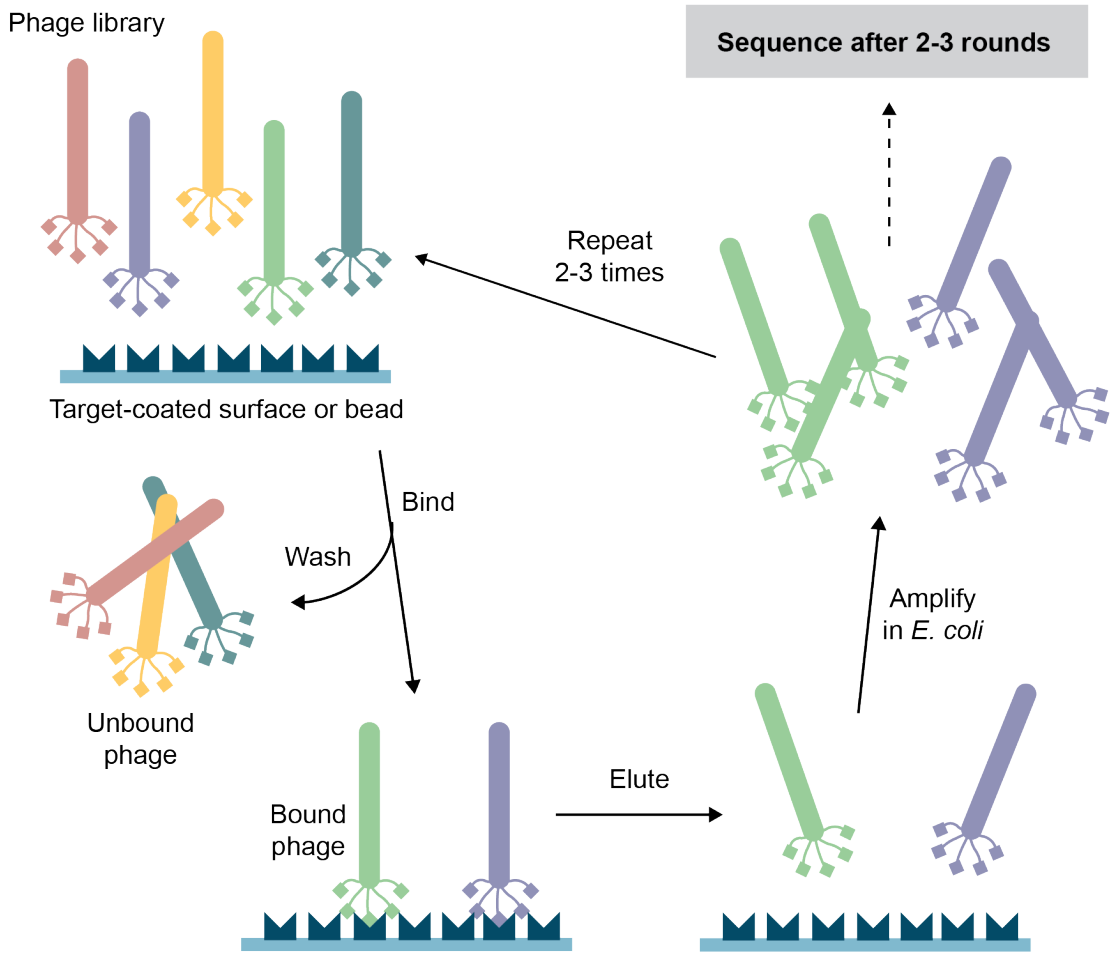

Figure 2. Generalized phage library preparation workflow. Phages displaying a diverse set of peptides are bound to a surface of interest. Unbound phages are washed away. Bound phages are eluted and amplified in *E. coli*. This cycle is repeated to enrich for phages specific to the surface of interest. Adapted from (*68*).

Chapter 2

Results

2.1 Phage display identifies a radiation-induced, tumor-specific peptide motif

To identify peptide sequences with high specificity, we panned a phage display library containing approximately 10^9 unique 12-mer polypeptide sequences displayed on the phage surfaces against irradiated and unirradiated GSCs, normal human astrocytes (NHAs), and neural stem cells (NSCs) (**Fig. 3, A and B**). Radioresistant populations were present in each tested cell line, albeit at different relative abundances (**Fig. 3C**). Importantly, to protect the surface presentation of glycoprotein modifications, cell-adhesion proteins, and other cell surface-displayed binding epitopes that could be influenced by dissociation, the phage display library was panned against whole, intact neurospheres. RNA-sequencing of amplified phages identified a number of phages with enriched binding in either irradiated or unirradiated cells in both tumor (GSC) and non-tumor (NHA and NSC) cell lines, including 88 phage sequences enriched in irradiated tumor and non-tumor cells and 6 sequences enriched in unirradiated groups (**Fig. 3D**). Furthermore, principle component analysis (PCA) of the bound phage sequences indicate that our radiation scheme does, indeed, induce significant changes in the surface molecular landscape of both tumor and non-tumor cell lines (**Fig. 3D**).

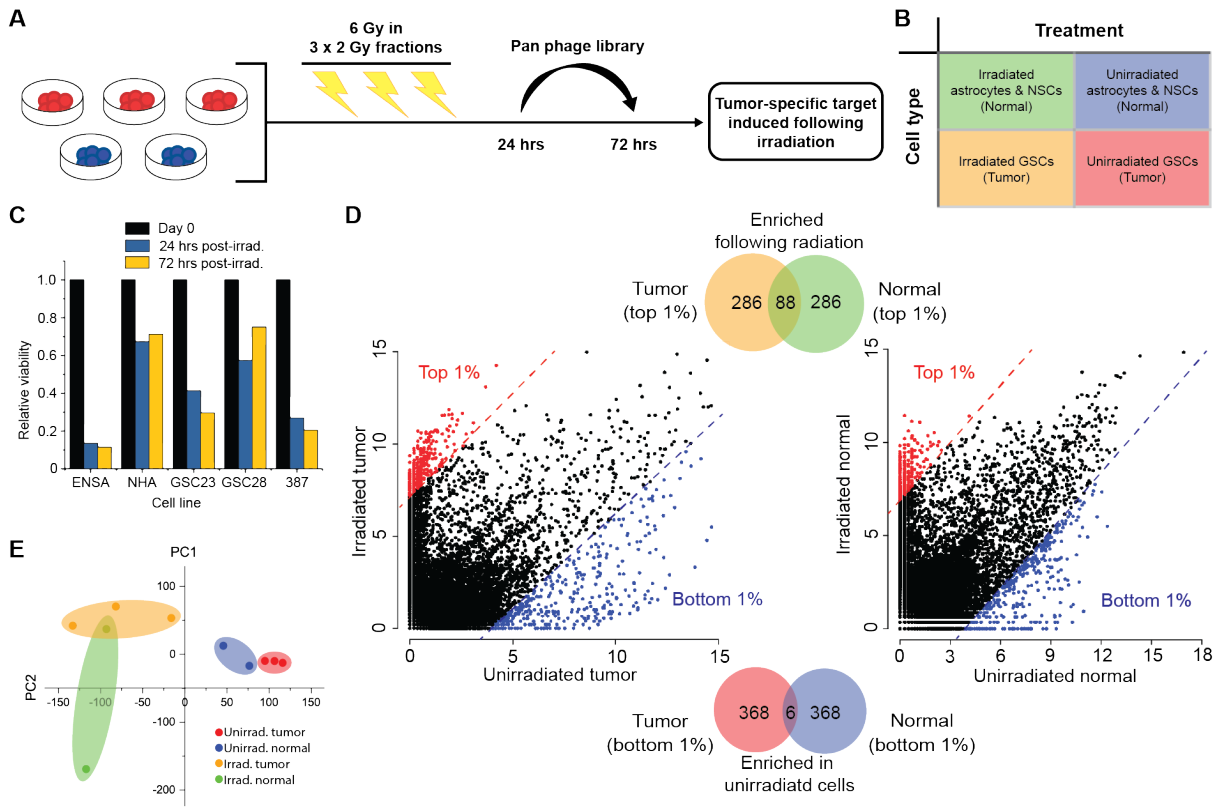

Figure 3. Phage display of unirradiated and irradiated tumor (GSCs) and normal (astrocytes and NSCs) cells. (**A**) Schematic of irradiation treatment paradigm and phage display panning in irradiated groups. The library was panned at 24 hours post-final irradiation, and enriched at 72 hours post-final irradiation. (**B**) Treatment groups and cell types that were panned against the phage display library. (**C**) Relative viability of astrocytes (ENSA), NHAs, and three patient-derived GSC lines (GSC23, GSC28, and 387) at 24 hrs and 72 hrs post-irradiation. (**D**) Volcano plots representing RNA-sequencing of enriched phages. Venn diagrams showing the number of these phage sequences enriched in unirradiated (bottom) and irradiated (top) cells for both tumor (left) and normal (right) cells. Overlaps represents the number of sequences with shared enrichment between tumor and normal cells. (**E**) PCA plot of the individual cell lines with and without radiation based on enriched phage sequences.

To identify highly specific for irradiated GSCs, we determined positive phage sequences as those that were bound to or internalized by irradiated GSCs and not bound to or internalized by non-tumor cells or unirradiated GSCs (**Fig. 4A**). Intersecting positively-identified sequences from three patient-derived GSC lines revealed two highly specific phage peptide sequences (YPHK-WHEFKQRV and WPLSRLVPPMES; **Fig. 4B**), and ranking all phage sequences based on overall binding specificity identified a single peptide (YPHKWHEFKQRV, referred to as "YPH-peptide")

with the highest enriched binding in irradiated GSCs (**Fig. 4, C and D**).

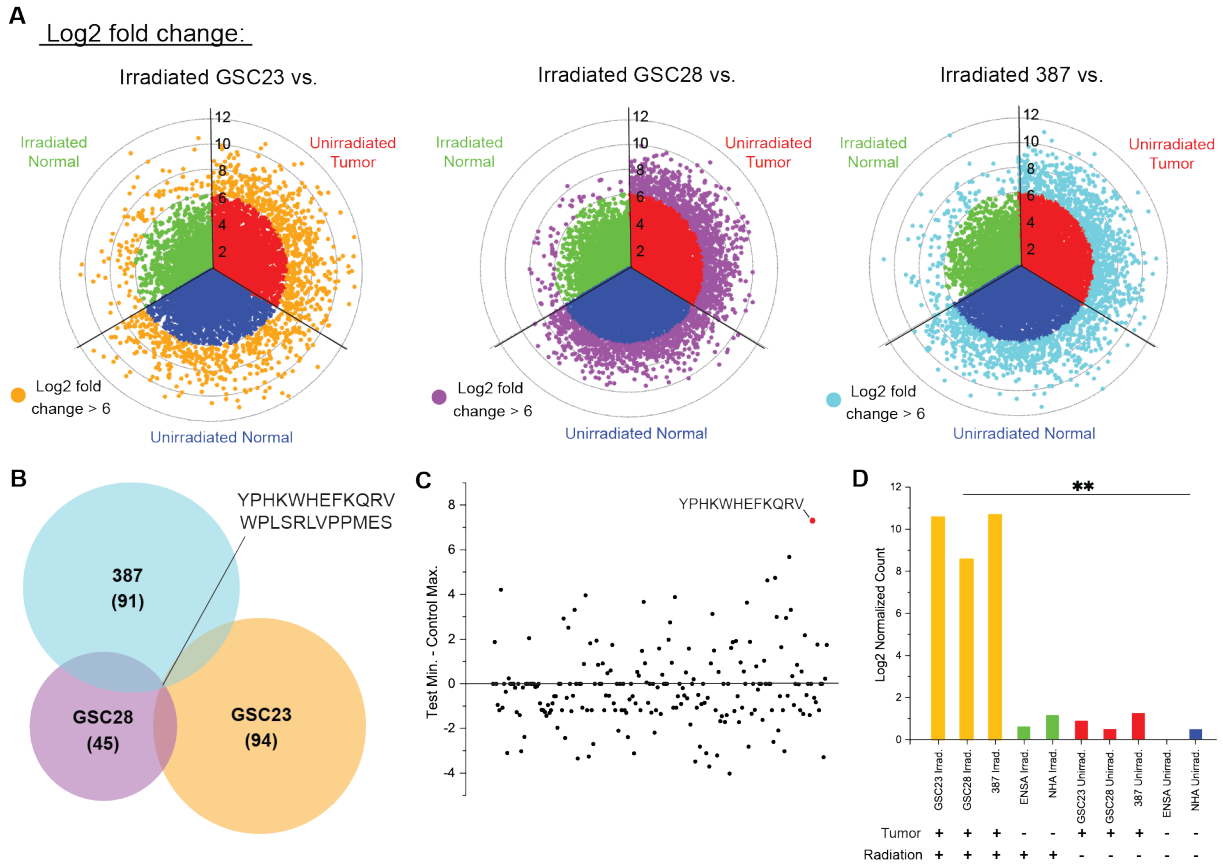

Figure 4. Identification of peptide sequences with binding specificity to irradiated GSCs. (**A**) Polar scatter plots of phage sequences identified with RNA-sequencing. Points in orange, purple, and cyan represent sequences with over 64-fold enrichment in irradiated GSCs (GSC23, GSC28, and 387, respectively) compared to their respective group. (**B**) Venn diagram showing the number of enriched sequences in each GSC line. Two peptide sequences (shown) are present in all lines. (**C**) Scatter plot of lowest observed specificities of all enriched sequences for irradiated GSCs. Values are calculated based on the difference in RNA-sequencing counts from the lowest irradiated GSC group and the highest from the other groups. The top sequence is highlighted in red. (**D**) RNA-sequencing counts of the top sequence, YPHKWHEFKQRV, across all groups. One-way ANOVA was used for statistical test, $^{**}P<0.01$.

2.2 Target peptide binds to irradiated tumor cells

Following identification of a phage peptide sequence that specifically binds to irradiated GSCs, we next sought to validate this preferential binding phenomenon in vitro using fluorescently-conjugated YPH-peptide. We found that a number of patient-derived GSC lines exhibit an increase

in peptide binding per viable cell following irradiation (i.e. increased binding in alive, radioresistant cells) (**Fig. 5A, left**). Interestingly, GSC lines that were more sensitive to ionizing radiation (GSC23 and 387) exhibited increased relative and overall peptide binding in radioresistant cells, while more radioresistant GSC lines (MES20 and 738) did not (**Fig. 5A**). These findings suggest that the YPH-peptide may bind specifically to a protein only present following irradiation and that the expression of this protein may allow a subset of GSCs to acquire acute radioresistance.

To interrogate the specificity of the YPH-peptide, we tested the relative binding of either the YPH-peptide or a scrambled control (FKQVHPHYKEWR, "scramble") in several unirradiated and irradiated GSC lines at different peptide concentrations. Consistent with previous results, GSC lines that display overall impaired resistance to acute death caused by ionizing radiation (**Fig. S1, A-C**) generally displayed increased relative YPH-peptide binding after irradiation compared to unirradiated YPH-peptide and irradiated scramble groups (**Fig. 5**B). Decreasing the peptide concentration decreased the relative peptide binding in a dose-dependent manner while also maintaining the highest levels in the irradiated group treated with YPH-peptide (**Figs. 5C and S1**). These trends were observed across all tested cell lines, independent of inherent radioresistance. Interestingly, the irradiated 387s (the most radio-vulnerable GSC line) displayed a completely different dose response to the YPH-peptide from all other GSC lines (**Fig. 5**C), supporting the high specificity of the YPH-peptide in this cell line.

Figure 5. YPH-peptide binding specificity in irradiated GSCs. (**A**) Relative survival (left) and relative peptide binding (right) of several unirradiated and irradiated GSC lines, ordered from highest survival to lowest ($n = 6$). (**B**) Relative peptide binding of several unirradiated and irradiated GSCs with either the YPH-peptide or a scrambled control, ordered from highest survival to lowest ($n = 4$). (**C**) Relative peptide binding dose response curves of GSC lines presented in (**B**) ($n = 4$). (**D**) *In vivo* radiation dosing and tumor growth experimental setup. (**E**) Representative image of harvested tumors from unirradiated (left) and irradiated (right) mice dosed with 400 μM YPH-peptide. Metric is 1 cm. (**F**) Fluorescent whole body and *ex vivo* tumor IVIS images of the YPH-peptide using a Cy5.5 excitation/emission channel (640 nm/700 nm) from mice dosed with 400 μM YPH-peptide. Tumors are matched (left to right) with the mice above. (**G**) Quantification of *ex vivo* fluorescence signal per gram tumor in unirradiated and irradiated mice at two peptide dosing concentrations ($n = 5$). Two-way ANOVA was used for statistical test unless otherwise stated, $^{*}P<0.05$, $^{***}P<0.001$, $^{***}P<0.001$, $^{****}P<0.0001$. Abbreviations are unirradiated (unirrad.) and irradiated (irrad.).

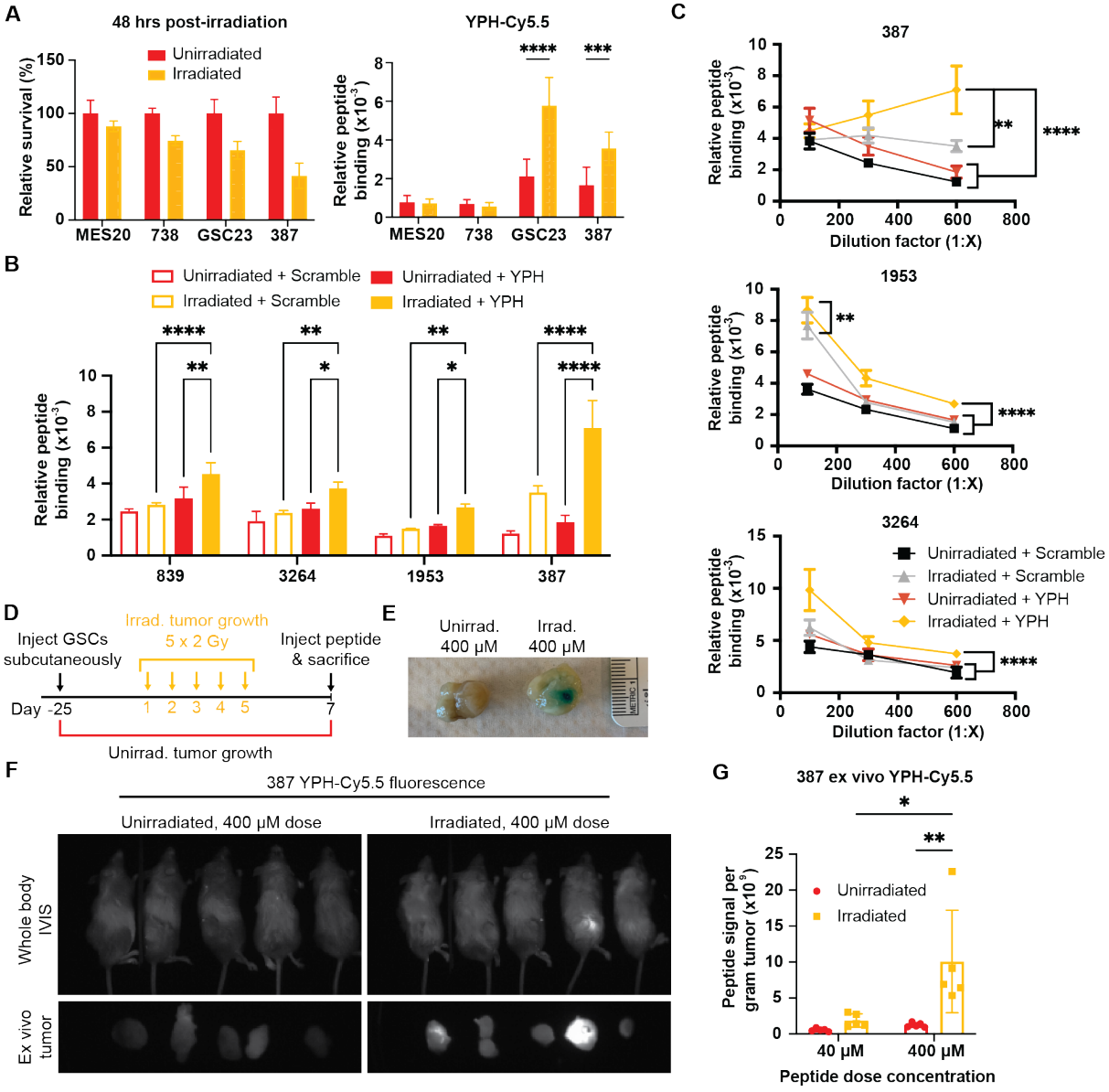
A
48 hrs post-irradiation
Unirradiated
Irradiated
Relative survival (%)
MES20
738
GSC23
387
YPH-Cy5.5
Relative peptide binding (x10-3)
****
***
B
Unirradiated + Scramble
Irradiated + Scramble
Unirradiated + YPH
Irradiated + YPH
Relative peptide binding (x10-3)
839
3264
1953
387
C
387
1953
3264
Relative peptide binding (x10-3)
Dilution factor (1:X)
Unirradiated + Scramble
Irradiated + Scramble
Unirradiated + YPH
Irradiated + YPH
D
Inject GSCs subcutaneously
Irrad. tumor growth
5 x 2 Gy
Inject peptide & sacrifice
Day -25
1 2 3 4 5
7
Unirrad. tumor growth
E
Unirrad. 400 µM
Irrad. 400 µM
F
387 YPH-Cy5.5 fluorescence
Unirradiated, 400 µM dose
Irradiated, 400 µM dose
Whole body IVIS
Ex vivo tumor
G
387 ex vivo YPH-Cy5.5
Peptide signal per gram tumor (x10 9)
Unirradiated
Irradiated
40 µM
400 µM
Peptide dose concentration

To validate the specificity of the YPH-peptide in vivo, we injected peptide at two different doses in unirradiated and irradiated immunocompromised mice bearing subcutaneous flank tumors of patient-derived GSCs (**Figs. 5D and S2**). While there is statistically non-significant trend of increased radiation-induced YPH-peptide binding in the low-dose regimes, the irradiated high-dose cohort had significantly increased peptide binding compared to both the unirradiated and low-dose cohorts (**Fig. 5, E-G**). Together, these findings indicate a dose-dependent specificity of the peptide following irradiation.

2.3 YPH-peptide may bind to aberrantly translocated proteins following irradiation

Because the YPH-peptide was identified using radioresistant, intact GSC-derived neurospheres, we hypothesized that the peptide could be binding to a protein that may be differentially present in intact neurospheres compared to single-cell GSC suspensions. Indeed, treatment with a dissociation agent abrogated the effect of radiation on relative peptide binding (**Fig. 6A**).

We next sought to interrogate possible internalization pathways that may result from novel, radiation-induced translocation to and from the plasma membrane, which could explain the specificity of the YPH-peptide. Using the cell lysate of irradiated GSCs, we performed immunoprecipitation followed by mass spectrometry (IP-MS) (**Fig. 6B**) and identified 14 proteins that bound specifically to the YPH-peptide compared to the scrambled control. Based on literature publications interrogating radioresistance, we further narrowed down these targets to four intracellularly expressed proteins which may be important for survival and be aberrantly translocated following irradiation (**Fig. 6B**): Ezrin (EZR), Radixin (RDX), Moesin (MSN) and Metadherin/Protein LYRIC (MTDH).

Figure 6. Radiation-induced binding of YPH-peptide to GSC-specific proteins. (**A**) Relative YPH-peptide binding of two GSC lines with and without mild dissociation into single-cell suspensions ("Diss." and "Whole," respectively) prior to peptide incubation. (**B**) IP-MS workflow. YPH-peptide was bound to irradiated GSC lysate and precipitated. Non-specific proteins were first eluted with the scrambled peptide. Shown are the 14 genes identified from the MS that are specific for the YPH-peptide. Shown (far-right) are the four candidate genes from the previous list that are implicated in radioresistance based on published data. (**C**) Relative mRNA fold-changes of each of the four genes in two GSC lines normalized to GAPDH, using qPCR (n = 3). (**D**) Western blot analysis depicting expressed protein levels of the four candidate genes with and without irradiation normalized to total loaded protein. Protein levels of a housekeeping gene (GAPDH) are shown below. (**E**) Representative fluorescent images of expression of the four candidate genes in unpermeabilized GSCs with and without irradiation. Scale bars are 150 μm for each group of images. (**F**) Fluorescence signal quantification per cell of the four genes in permeabilized (perm.) and unpermeabilized (unperm.) GSCs (n >3). (**G**) Flow cytometry of surface expression of the four candidate genes in unpermeabilized unirradiated (top) and irradiated (bottom) GSCs (n = 10^5). (**H**) Quantifications of the ratio of $FITC^+/PE\text{-}YG^-$ cells to $PE\text{-}YG^-$ cells in (**G**) for each gene (n = 3). Two-way ANOVA was used for statistical test unless otherwise stated, $^*P<0.05$, $^{***}P<0.001$, $^{***}P<0.001$, $^{****}P<0.0001$. Abbreviations are dissociated (diss.), unirradiated (unirrad.), irradiated (irrad.), fluorescence (fluor.).

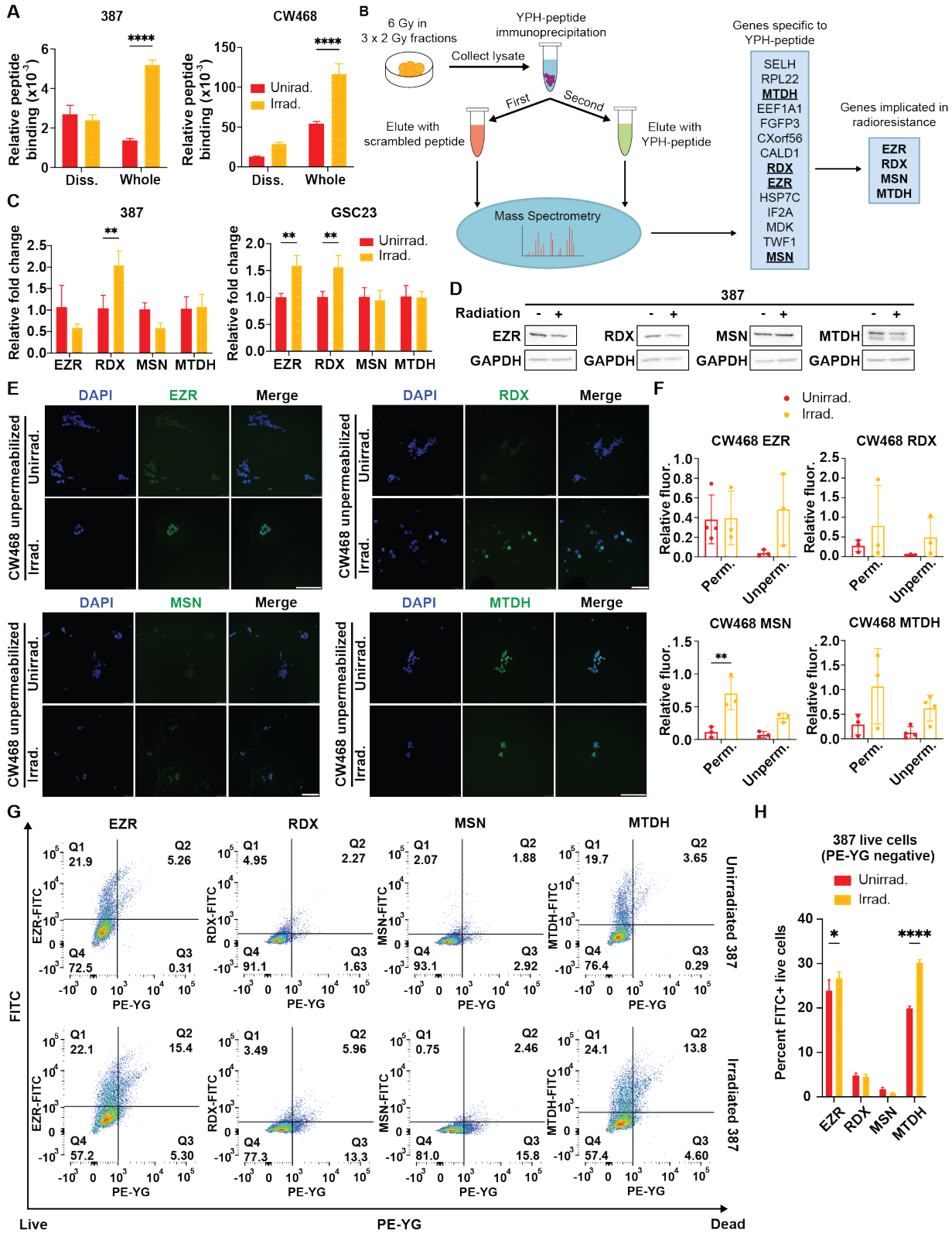
A
387
CW468
Relative peptide binding (x10-3)
Diss.
Whole
Unirad.
Irrad.
****
B
6 Gy in 3 x 2 Gy fractions
Collect lysate
YPH-peptide immunoprecipitation
First
Second
Elute with scrambled peptide
Elute with YPH-peptide
Mass Spectrometry
Genes specific to YPH-peptide
SELH
RPL22
MTDH
EEF1A1
FGFP3
CXorf56
CALD1
RDX
EZR
HSP7C
IF2A
MDK
TWF1
MSN
Genes implicated in radioresistance
EZR
RDX
MSN
MTDH
C
387
GSC23
Relative fold change
EZR
RDX
MSN
MTDH
Unirrad.
Irrad.
**
D
387
Radiation
EZR
RDX
MSN
MTDH
GAPDH
E
DAPI
EZR
RDX
MSN
MTDH
Merge
CW468 unpermeabilized
Unirrad.
Irrad.
F
Unirrad.
Irrad.
CW468 EZR
CW468 RDX
CW468 MSN
CW468 MTDH
Relative fluor.
Perm.
Unperm.
G
EZR
RDX
MSN
MTDH
FITC
PE-YG
Q1
Q2
Q3
Q4
21.9
5.26
72.5
0.31
4.95
2.27
91.1
1.63
2.07
1.88
93.1
2.92
19.7
3.65
76.4
0.29
22.1
15.4
57.2
5.30
3.49
5.96
77.3
13.3
0.75
2.46
81.0
15.8
24.1
13.8
57.4
4.60
Unirradiated 387
Irradiated 387
Live
Dead
H
387 live cells (PE-YG negative)
Unirrad.
Irrad.
Percent FITC+ live cells
*
****
EZR
RDX
MSN
MTDH

One explanation for the increased YPH-peptide binding in irradiated GSCs may be upregulation of one or more of these four genes at either the mRNA or protein level. We performed quantitative PCR (qPCR) and western blots of unirradiated and irradiated GSCs to determine the effect of irradiation on relative mRNA and protein levels, respectively, of these four genes. While we observed statistically significant differences in relative mRNA levels (**Fig. 6C**), these differences did not correlate with changes at the protein level (**Fig. 6D**) and, subsequently, do not fully explain the several-fold increase in peptide binding observed after irradiation (**Fig. 5, A and H**).

We next hypothesized that the increase in YPH-peptide binding could also be due to aberrant translocation of one or more of these proteins following irradiation. All four genes showed a general trend towards an increased surface expression based on relative intensities from immunofluorescence (IF) images of unpermeabilized GSCs (**Fig. 6, E and F**). To corroborate these findings, we performed flow cytometry to visualize and quantify the effect of radiation on plasma membrane surface presentation of these proteins. We observed a modest increase in EZR presentation and a pronounced increase in MTDH presentation (**Fig. 6, G and H**), indicating that both EZR and MTDH may be aberrantly translocated to the cell surface following irradiation.

2.4 EZR combinatorially inhibits GSC growth after irradiation

To determine the importance of these four genes in GSCs, we performed shRNA-mediated knockdown and CRISPR-mediated knockout in unirradiated GSCs using two targeted shRNA sequences and four sgRNA sequences per gene. CRISPR-knockout of the target genes significantly reduced proliferation (**Fig. 7A**) compared to a non-targeting control (sgCONT). shRNA-mediated knockdown also yielded comparable reductions in proliferation (**Fig. 7B**), suggesting that all four genes may be important for unirradiated GSC growth. We next sought to interrogate the roles of these genes in supporting radioresistance. We observed two forms of acute vulnerability to radiation in our patient-derived GSC lines. Firstly, GSCs may be subject to stresses such as DNA damage and ROS generation (*32*, *46*) which can lead directly to acute cell death. Secondly,

cells that survive these radiation-induced stresses experience a reduced ability to proliferate in the acute period following. Interestingly, both RDX- and MSN-knockdown GSCs had comparable or better resistance to radiation-induced death than a non-targeting control, while survival in EZR- and MTDH-knockdowns was significantly reduced (**Fig. 7C**). Comparing knockdowns with and without irradiation, EZR-knockdowns had greater growth impairment after irradiation, while RDX-knockdowns had much less impairment (**Fig. 7D**). Only EZR knockdown impaired unirradiated growth, irradiated growth, and radioresistance.

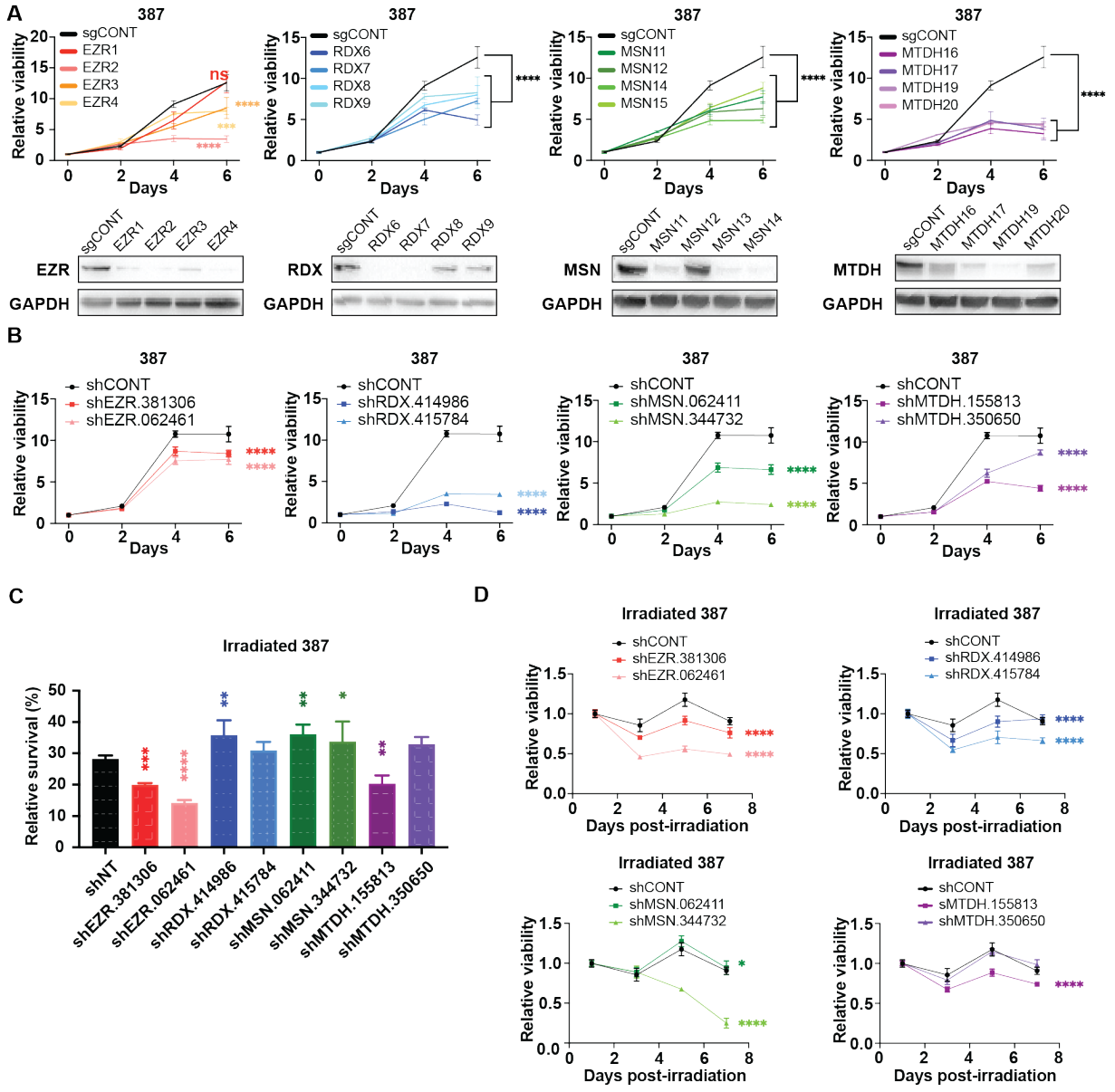

Figure 7. Synthetic perturbation of ERM proteins and MTDH expression in GSCs. (A) Relative growth (top) of CRISPR-mediated knockouts of the four genes in GSCs without irradiation ($n = 3$) and their associated western blots confirming protein knockout (bottom) using four different guides per gene. Significance is compared to sgCONT. (**B**) Relative growth of shRNA-mediated knockdowns of the four genes in GSCs without irradiation ($n = 6$) using two sequences per gene. Significance is compared to shCONT. (**C**) Relative survival at 48 hours post-irradiation of GSCs after shRNA-mediated knockdown ($n = 6$). One-way ANOVA was used for statistical test, $*P<0.05$, $**P<0.01$, $***P<0.001$, $****P<0.0001$. (**D**) Relative growth of irradiated GSCs following shRNA-mediated knockdowns of the four genes ($n = 6$). Significance is compared with shCONT. Two-way ANOVA was used for statistical test unless otherwise stated, $*P<0.05$, $***P<0.001$, $****P<0.0001$.

Chapter 3

Discussion

While concomitant chemotherapy and radiotherapy are the standard-of-care in GBM treatment, recurrence is inevitable due to the presence of subsets of chemoresistant and radioresistant GSCs which evade treatment and repropagate the tumor (*30*, *32*, *69*). Higher inherent radioresistance in GSCs suggests a unique molecular response to ionizing radiation that is absent in both non-tumor and non-stem tumor cells, and thus, may be a molecular vulnerability. We used phage display to identify two 12-mer polypeptides which have highly enriched cell surface binding in patient-derived GSCs and show that the top candidate peptide, YPHKWHEFKQRV, binds preferentially to irradiated GSCs. While the YPH-peptide did not have increased binding in every irradiated patient-derived GSC line tested, this may be a result of cellular heterogeneity between the different cell lines (e.g. glioma subtype). Furthermore, we observed different levels of innate radioresistance between cell lines, which also seemed to correlate roughly with the ability to preferentially bind the peptide after irradiation. In particular, two classically-subtyped patient-derived GSC lines (387 and CW468) seemed to be the most vulnerable to ionizing radiation, yet yielded some of the greatest increases in peptide binding following irradiation. Moreover, irradiated 387s had a completely different peptide binding dose response from any of the other tested cell lines, suggesting that there may be some unique biology occurring in either this GSC line or in radio-vulnerable GSC lines.

Of particular concern is whether cell death affects peptide binding. While it does appear that more radio-vulnerable GSC lines are more specific for the YPH-peptide following irradiation, this also raises the possibility that the peptide is binding non-specific cellular debris from dead cells.

Indeed, we acknowledge this possibility which stems from the difficulty in defining and isolating neurospheres of "live" cells, yet assert the specificity of the YPH-peptide for live, irradiated GSCs based on the presented evidence. We have shown that the peptide has considerable binding compared to a scrambled control and that its binding levels are concentration-dependent. Critically, the peptide's preferential binding is abrogated by treatment with a mild dissociation agent immediately prior to peptide incubation, implicating that a significant amount of binding occurs separate from non-specific association with cellular debris.

While there is not yet enough evidence to clearly indicate with what this binding occurs, it is possible that specific cleavable extracellular domains (e.g. glycosylations) or physical cell-cell contact may be required. We identified four intracellularly annotated proteins which bind the YPH-peptide following irradiation, may be aberrantly translocated to the plasma membrane following irradiation, and are implicated in supporting radioresistance of GSCs. Importantly, both EZR and MTDH showed increased cell surface presentation following irradiation in radioresistant cells. While there are discrepancies in the changes in surface presentation observed between IF and flow cytometry (**Fig. 6, E-H**), these likely result from the sampling variance in IF compared to large sample sizes in flow cytometry, different primary antibody incubation times, and the quantification method used in IF which is strictly an approximation of relative fluorescence.

EZR is canonically association with the actin cytoskeleton on the cytoplasmic side of the plasmid membrane (*70*, *71*). It binds CD44—an important cancer stem cell surface marker—and through its interaction with EBP50 (ERM-binding phosphoprotein 50) is involved in internalization of various plasma membrane proteins including platelet-derived growth factor receptor (PDGFR), an important oncogenic receptor tyrosine kinase (*70*). Indeed, these evidence suggest mechanisms both for aberrant membrane presentation of EZR and for its role in supporting GSC maintenance. On the other hand, MTDH primarily localizes to the nucleus, perinuclear region, and endoplasmic reticulum, except when it associates with tight junctions in endothelial cells, and its surface expression is very low in the brain (*57*, *72*, *73*). It contains a single transmembrane domain and an activating domain for NF-B (*74*), a key oncogenic transcription factor, suggesting an exosome-based

plasma membrane translocation mechanism and also a role in GSC maintenance. To our knowledge, these are the first implications of aberrant cell surface presentation of either of these proteins, both of which are intracellularly annotated. Thus, radiation-induced translocation of EZR or MTDH may act as a radioresistance mechanism in surviving GSC populations.

Interestingly, significantly reduced proliferation in both CRISPR-knockouts and shRNA-mediated knockdowns indicate that all four candidate genes may be essential for unirradiated GSC growth. When cells were dosed with ionizing radiation, EZR and MTDH knockdown both significantly reduces survival, supporting our hypothesis that aberrant translocation of these genes may confer increased radioresistance. Additionally, proliferation in EZR knockdowns seemed to be combinatorially affected by radiation, further implicating a role for EZR in radioresistance. However, it is still unclear to what extent radiation-induced death factors into this combinatorial growth impairment, and the inability to completely decouple the proliferation reduction and the survival changes is a key limitation of these analyses which should be addressed further in future studies.

Nevertheless, we have shown the specificity of the YPH-peptide for irradiated GSCs, independent of the identity of its binding partner, implicating its use in possible targeted therapeutics. Several studies have validated the use of homing peptides in tumor-targeting nanoparticles (*75*, *76*), and many classes of peptide-modified nanoparticles have the advantage of being both intravenously injectable and blood-brain-barrier permeable (*77*, *78*). Of particular excitement are the implications for this peptide and other phage-display-identified peptides in CAR T cell therapies. CAR T therapy is a promising field in GBM treatment due to the immunosuppressive nature of the tumor (*79*, *80*), and there are several ongoing clinical trials assessing the safety and efficacy CAR T cells targeting GBM-enriched surface markers (e.g. EGFR) (*81–83*). Critically, two key considerations in designing CARs are the preferential expression of the target antigen in tumors and the surface presentation of this antigen (*79*, *80*), and we have shown the YPH-peptide fulfills both of these criteria, highlighting its clinical feasibility as a GBM-targeting, radiation co-therapy.

Chapter 4

Materials and Methods

4.1 Cell culture

Patient-derived GSCs were cultured as neurosphere suspensions in Neurobasal medium (NBM) supplemented with 1% L-glutamine, 1% sodium pyruvate, 2% B27, 10 ng/mL basic human fibroblast growth factor (bFGF), 10 ng/mL human epidermal growth factor (EGF), and 1% penicillin/streptomycin.

4.2 In vitro irradiation

GSCs were dissociated into single-cell suspensions with Accutase (Innovative Cell Technologies #AT104), and plated the day prior to irradiation. Each plate was subjected three times to ionizing radiation at doses of 2 Gy each (for a total of 6 Gy), with 48 hours of rest between each dose (e.g. MWF dose with Tuesday and Thursday rest). GSCs were dissociated once more the day before the final administration dose (e.g. Thursday).

To measure fluorescently-conjugated peptide binding, a slightly different radiation schedule was used due to pandemic-associated facility restrictions. GSCs were dissociated and plated the day prior to irradiation, and dosed twice at doses of 3 Gy each (for a total of 6 Gy) , with 48 hours of rest between the two doses (e.g. MW dose with Tuesday rest).

4.3 Phage display screen

Phage-competent bacteria, ER2738, were maintained, prepared and amplified according to manufacturer's instruction. Cells used in the screen were either unirradiated or irradiated with 6 Gy fractionated across 3 doses (MWF). Cells were passaged on the day prior to the last dose of radiation and maintained as spheres for all subsequent experiment to avoid cleaving cell-surface glycoproteins or modifications. 24 hours after the final dose of radiation, half the cells were centrifuged at 300 rpm for 3 minutes to remove single dead cells. Phage display screening was then performed using 10 μL of the NEB Phage Display Ph.D.-12 library with a modified version of this protocol: https://www.ncbi.nlm.nih.gov/pmc/articles/PMC4053471/. First, cells were incubated in blocking solution (1% BSA in neurobasal media without additives) for one hour, shaking, on ice. 10 μL of the phage library was added to each sample and incubated for 2 hours on a shaker at room temperature. Cells were then washed 5 times in 0.1% BSA in NBM and eluted with 0.1 M HCl-Glycine, 0.9% NaCl pH 2.2. Cells were then lysed in with RIPA buffer with EDTA to release phage that had been internalized during the incubation period. Lysate and eluted phage were then added to ER2738 bacteria in early-log growth phase. The phage-bacteria mixture was amplified by incubation for 4.5 hour at 37 °C and phage were precipitated and titered according to manufacturer's instructions. The phage amplified from the 24-hour samples were subsequently used in panning against the remaining cells at 72-hours after irradiation (and the equivalent timing in control, unirradiated samples). Panning was repeated at this time point and the resulting phage were amplified and processed for sequencing.

4.4 Sequencing and Analysis

DNA was isolated from phage and samples were prepared for sequencing on the Illumina MiSeq platform according to manufacturer instructions. Samples were multiplexed for sequencing to achieve at least 1 million reads per sample. MiSeq data for each condition were aligned to the NEB phage display library using PHASTpep with the kind assistance of Dr. Lindsay Brinton

(https://pubmed.ncbi.nlm.nih.gov/27186887/). PHASTpep identifies the common peptide flanking sequences and extracts the variable DNA sequence between them, then converts the DNA sequence into the corresponding peptide sequence and counts the frequency for each peptide sequence. Peptide frequencies were normalized to the total read count for each sample and transformed to Log2(counts + 1) for downstream analyses.

4.5 In vitro peptide binding assay

GSCs were irradiated as previously described. Forty-eight hours post-irradiation, both unirradiated and irradiated GSCs were pelleted through centrifugation at 500 rpm (20-25 rcf) for 3 mins to isolate live cells. If necessary, these cells were dissociated with Accutase. An appropriate number of cells were resuspended in 150 μL complete NBM containing either FAM-conjugated YPH-peptide (AnaSpec), Cy5.5-conjugated YPH-peptide (LifeTein), or Cy5.5 conjugated scrambled peptide (LifeTein) at an appropriate concentration, and were incubated at 37°C for 1 hr in dark. Cells were pelleted on a benchtop centrifuge at 500 rcf for 5 mins, followed by repeated washing and centrifugation three times with PBS. Cells were resuspended in an appropriate amount of PBS and plated on 96-well clear bottom assay plates at 50 μL of suspension per well. Fluorescence was measured on a fluorescent microplate reader (Tecan) for FAM (ex. 488/9 nm, em. 530/20 nm) and Cy5.5 (ex. 675/10 nm, em. 710/20 nm). Cell viability was measured by adding 50 μL of Cell Titer GLO (Promega #G7570) to each well, gently swirling for 5 mins, and measuring luminescence on a luminescent microplate reader. Relative peptide binding was calculated as the ratio between fluorescence signal and luminescent signal for each well.

4.6 Cell survival assay

GSCs were dissociated and plated (2000 cells/well, 35 μL/well) one day prior to irradiation. Cells were irradiated as described previously. Forty-eight hours post-irradiation, 35 μL of Cell Titer GLO was added to each well, followed by gentle swirling for 5 mins, and measurement of luminescence by a luminescent microplate reader. Relative survival was calculated as the ratio

between the luminescence of irradiated and unirradiated plates.

4.7 Cell growth assay

GSCs were dissociated and plated at Day 0 (2000 cells/well, 35 μL/well). Cell Titer GLO (35 μL) was added to each well, followed by gentle swirling for 5 mins, and measurement of luminescence by a luminescent microplate reader. This was repeated for Days 2, 4, and 6. Relative viability was calculated by normalizing the luminescence values to the Day 0 average for each experimental group.

4.8 *In vivo* luciferase and peptide binding assays

GSCs were infected with luciferase-containing lentiviruses. Prior to injection, cells were dissociated and counted. Nude mice were split into four groups (n = 5) and subcutaneously injected with 19 million cells (200 μL) in the right flank. Visible tumors were allowed to form beneath the skin. Tumors were irradiated five consecutive days at doses of 2 Gy each, with 24 hours of rest between each dose. Forty-eight hours after the final irradiation dose, D-luciferin (Sigma) was injected intraperitoneally (i.p.) (33.33 g/mL, 50 μL) and allowed to circulate for 10 mins. Luminescence was measured with IVIS (In Vitro Imaging System) with 10 seconds of exposure. Mice were i.p. injected with either 40 μM or 400 μM of Cy5.5 conjugated YPH-peptide in PBS (100 μL). The peptide was allowed to circulate for 30 minutes, followed by fluorescence imaging with IVIS (ex. 640 nm, em. 700 nm, 1 second exposure). Mice were euthanized, and tumors were harvested and weighed. Fluorescence of harvested tumors was measured with IVIS. Tumors were fixed in 4% paraformaldehyde followed by exchange in 30% sucrose.

4.9 IP-MS

Approximately 200 million GSCs were collected to perform IP-MS. Spheres were irradiated with 6 Gy fractionated over 2 doses with one recovery day in between radiation doses. 48 hours after the second dose of radiation, cells were collected and centrifuged at 600 RPM for 3 minutes, then

snap frozen at -80 °C. Pellets were lysed in 2 mL tissue lysis buffer (50 mM Tris-Cl pH 8.5, 200 mM n-Octyl-beta-D-glucopyranoside, 5 mM EDTA pH 8.5 and EDTA-free protease inhibitor (Roche)). Cells were resuspended in lysis buffer and passed sequentially through needles of progressively smaller gauge, then incubated at 4 °C for 2 hours with rotation. Lysate was spun at 14000 rpm for 15 min at 4 °C, supernatant was collected and incubated with peptide-conjugated magnetic beads overnight with rotation at 4 °C. Neutravidin Sera-Mag Speedbeads were blocked with 2% BSA and 0.02% Tween-20 in PBS for 15 min at room temperature, washed three time in PBST/BSA and twice more in PBST,. Beads were then incubated with 0.8 mM of peptide for 30 minutes shaking at room temperature, washed twice in 0.025% Tween-20 in PBS and finally washed twice with tissue lysis buffer. After overnight incubation, beads were washed 8 times in wash buffer (25 mM Tris-Cl pH 8.0, 75 mM n-Octyl-beta-D-glucopyranoside, 1 mM MnCl2, 1 mM MgSO4, 1 mM CaCl2 and 1 tablet of EDTA-free protease inhibitor. Beads were then washed 3 times with 0.55 mM of FAM-scramble control peptide resuspended in wash buffer. Bound protein was eluted with 1 mM FAM-peptide in wash buffer in 4 washes. The final eluate and the control eluate (eluted with FAM-scramble control) were sent for mass spectrometry. Proteins enriched at FDR $<$0.05 in the test vs control sample were considered to be specifically bound to the peptide.

4.10 Quantitative PCR

RNA was isolated using a Direct-zol RNA Miniprep kit (Zymo) according to the manufacturer's instructions. Purified RNA was quantified with a Nanodrop spectrophotometer. RNA was reverse transcribed to cDNA using a High-Capacity Reverse Transcription kit (Invitrogen). cDNA was diluted appropriately and analyzed with real-time PCR with the relevant primers (**Table S1**) using PowerUp SYBR Green Master Mix (Invitrogen) according to the manufacturer's instructions. Primers were designed using PrimerBank (*84*, *85*).

4.11 Western blots

Cells were pelleted by centrifugation at 2000 rcf for 5 mins at 4°C and resuspended in an appropriate volume of RIPA buffer (Sigma). This suspension was briefly vortexed and centrifuged at 14000 rcf for 15 mins at 4°C to pellet cellular debris. The supernatant was collected and the protein concentration was quantified with a Pierce BCA Protein Assay kit (Thermo Scientific) according to the manufacturer's instructions. Samples were stored at -80°C. Equal quantities and volumes of sample were loaded into wells of a 10% polyacrylamide denaturing gel, and a voltage was applied (90V for 10 mins followed by 110V for 50 mins). The gel was transferred to a nitrocellulose membrane at 300 mA for 90 mins at 4°C. Blots were washed in TBST, blocked with 5% milk and incubated at 4°C overnight in blocking buffer containing primary antibody. EZR (Cell Signaling Technologies #3145), RDX (Cell Signaling Technologies #2636), MSN (Cell Signaling Technologies #3150), MTDH (Cell Signaling Technologies #14065), and GAPDH (Cell Signaling Technologies #2118) antibodies were used at 1:1000 dilutions. Blots were incubated in blocking buffer containing an appropriate horse radish peroxidase (HRP)-linked secondary antibody for 1 hour at room temperature. HRP substrate was added, and the blots were imaged on a ChemiDoc (Bio-Rad). Blots were stripped with stripping buffer (Thermo Scientific #21059) to allow re-imaging with different antibodies.

4.12 Immunofluorescence imaging

Irradiated GSCs were plated onto glass cover slips coated with Matrigel (Corning #344277) immediately following radiation. Cells were allowed to attach and grow for 48 hours, followed by fixation in 4% paraformaldehyde. Cells were washed with PBS and blocked in 10% normal goat serum for 60 mins. EZR (Bioss #BS-1343R), RDX (Invitrogen #MA5-32213), MSN (Invitrogen #MA5-32231), and MTDH (Invitrogen #MA5-36100) antibodies were conjugated with a fluorescent dye using an antibody conjugation kit (Invitrogen #A20181) according to the manufacturer's instructions. Cells were incubated overnight in the dark in 10% goat serum containing the appro-

priate fluorescent antibody (1:50) and DAPI (1:1000), followed by incubation with an appropriate secondary antibody, if necessary. Cover slips were mounted onto microscope slides for imaging. DAPI was detected with excitation at 405 nm and antibodies were detected with excitation at either 488 nm or 568 nm.

4.13 Flow cytometry

Unirradiated and irradiated GSCs were pelleted at 500 rpm (20-25 rcf) for 3 mins, followed by dissociation and passage through a 0.2 μm filter. Cells were kept on ice for the remainder of the assay. Cells were incubated in 100 μL of FACS buffer (0.1% EDTA, 5% FBS, and 1% BSA in PBS) with the appropriate fluorescent antibody (1:50) and a live/dead stain (1:1000; Invitrogen #L34959) for 1 hour at 4°C in the dark. Cells were washed three times with FACS buffer and resuspended. Flow cytometry was performed on a BD LSRFortessa with FITC and PE-YG lasers, and compensation was performed using compensation beads (Invitrogen #01-3333-41). Data were analyzed in FlowJO.

4.14 CRISPR knockouts and shRNA knockdowns

CRISPR inserts were designed as shown in **Table S2**. shRNA sequences were designed to target the sequences shown in **Table S3**. CRISPR cloning was performed as described previously (*86*, *87*). Briefly, CRISPR guide spacers were designed using a validated platform from the Broad Institute (*88*, *89*). Modified spacer sequences were cloned into a CRISPR lentiviral vector and amplified in *E. coli*. Sequence insertion was confirmed with sequencing. Lentivirus was produced in HEK293T cells using 2nd-generation lentiviral packaging plasmids and polyethyleneimine as a transfection agent, harvested, and concentrated. For transfection, 7.5×10^5 GSCs were plated in single-cell suspension and lentivirus was added. The next day, media was refreshed with complete NBM and cells were allowed 24 hours for expression of antibiotic resistance markers. Selection was performed using the appropriate antibiotic. Knockout efficiency was evaluated with western blots. GSCs were assayed within one week after selection to ensure sufficient knockout.

Candidate shRNA sequences were determined using the platform from the Broad Institute. shRNA vectors were obtained as a plasmid-containing bacterial glycerol stock, and cloning and transfection were performed as with CRISPR lentiviral vectors. Knockdown efficiency was evaluated with qPCR. GSCs were assayed within one week after selection to ensure sufficient knockdown.

4.15 Statistical analysis

Statistical parameters are provided in each figure legend. Multiple group comparisons were compared with either one-way ANOVA with Dunnett's post-hoc analysis or two-way ANOVA with Tukey's post-hoc analysis (by GraphPad Prism). $P < 0.05$ was designated as the threshold for statistical significance. All data are displayed as mean values with error bars representing standard deviation.

Appendix A

Supplemental Tables

Table S1. qPCR primer sequences, listed from 5' end to 3' end.

Gene name	PrimerBank ID	Forward primer	Reverse primer
EZR	161702985c1	ACCAATCAATGTCCGAGTTACC	GCCGATAGTCTTTACCACCTGA
RDX	62244047c1	TATGCTGTCCAAGCCAAGTATG	CGCTGGGGTAGGAGTCTATCA
MSN	53729335c1	ATGCCCAAAACGATCAGTGTG	ACTTGGCACGGAACTTAAAGAG
MTDH	223555916c1	AAATGGGCGGACTGTTGAAGT	CTGTTTTGCACTGCTTTAGCAT
GAPDH	378404907c1	GGAGCGAGATCCCTCCAAAAT	GGCTGTTGTCATACTTCTCATGG

Table S2. CRISPR guide RNA insert sequences used for cloning, listed from 5' end to 3' end.

Sequence name	Target gene	Forward sequence	Reverse sequence
EZR1	EZR	CACCGTGCGGCGCATATACAACTCA	AAACTGAGTTGTATATGCGCCGCAC
EZR2	EZR	CACCGTGTGGCATGCGGAACACCGT	AAACACGGTGTTCCGCATGCCACAC
EZR3	EZR	CACCGCTTTATTATCCACATAGTGG	AAACCCACTATGTGGATAATAAAGC
EZR4	EZR	CACCGGAAGAAAAGGAGAGAAACCG	AAACCGGTTTCTCTCCTTTTCTTCC
RDX6	RDX	CACCGATGATAGACTCCTACCCCAG	AAACCTGGGGTAGGAGTCTATCATC
RDX7	RDX	CACCGATAAAAAAGGAACTGAATTG	AAACCAATTCAGTTCCTTTTTTATC
RDX8	RDX	CACCGCTCGTCTGAGAATCAATAAG	AAACCTTATTGATTCTCAGACGAGC
RDX9	RDX	CACCGCAGACAATTAAAGCTCAGAA	AAACTTCTGAGCTTTAATTGTCTGC
MSN11	MSN	CACCGGCACGGAACTTAAAGAGCAG	AAACCTGCTCTTTAAGTTCCGTGCC
MSN12	MSN	CACCGGGAACAGCACAAACTCAACA	AAACTGTTGAGTTTGTGCTGTTCCC
MSN14	MSN	CACCGCTTAGACTGGACAGCATACG	AAACCGTATGCTGTCCAGTCTAAGC
MSN15	MSN	CACCGCTCATAGATGTTGAGACCCA	AAACTGGGTCTCAACATCTATGAGC
MTDH16	MTDH	CACCGTGATGCGGTTGTAAGTTGCT	AAACAGCAACTTACAACCGCATCAC
MTDH17	MTDH	CACCGCTGGAGCCGAAACGGTACCC	AAACGGGTACCGTTTCGGCTCCAGC
MTDH18	MTDH	CACCGTACCACTTCTGATTATCAGT	AAACACTGATAATCAGAAGTGGTAC
MTDH20	MTDH	CACCGGAAAACCTCACTGTCAATGG	AAACCCATTGACAGTGAGGTTTTCC

Table S3. shRNA target sequences, listed from 5' end to 3' end.

Sequence name	Target gene	Clone ID	Target sequence
shEZR.381306	EZR	TRCN0000381306	CCGTGGGATGCTCAAAGATAA
shEZR.062461	EZR	TRCN0000062461	CGTGGGATGCTCAAAGATAAT
shRDX.414986	RDX	TRCN0000414986	GAAGCAACTTCAGGCATTAAG
shRDX.415784	RDX	TRCN0000415784	ATGAGCATGACGACAAGTTAA
shMSN.062411	MSN	TRCN0000062411	GCATTGACGAATTTGAGTCTA
shMSN.344732	MSN	TRCN0000344732	ACCACCGGGAAGCAGCTATTT
shMTDH.155813	MTDH	TRCN0000350650	CGTGATAAGGTGCTGACTGAT
shMTDH.350650	MTDH	TRCN0000155813	AGCCGTAATCAACCCTATATC

Appendix B

Supplemental Figures

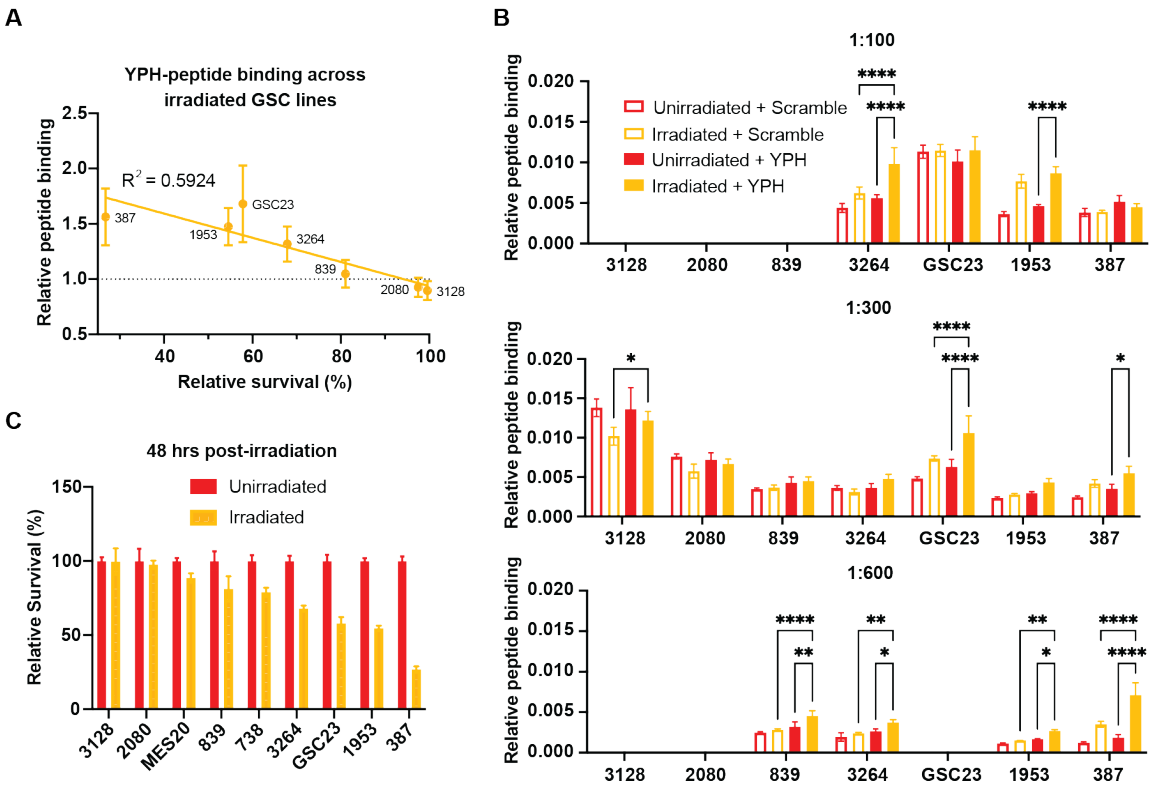

Figure S1. Comparison of peptide binding and radioresistance in GSCs. (**A**) Scatter plot of relative YPH-peptide binding across cell lines with varying levels of relative survival. Linear regression (solid line) and non-specific binding cut-off (dashed line) are shown. Points below the dashed line do not have increased YPH-binding. (**B**) Relative peptide binding of YPH-peptide and the scrambled control at different peptide concentrations for various GSC lines. (**C**) Relative survival of various GSC lines following irradiation. Two-way ANOVA was used for statistical test unless otherwise stated, *$P<0.05$, ***$P<0.001$, ***$P<0.001$, ****$P<0.0001$.

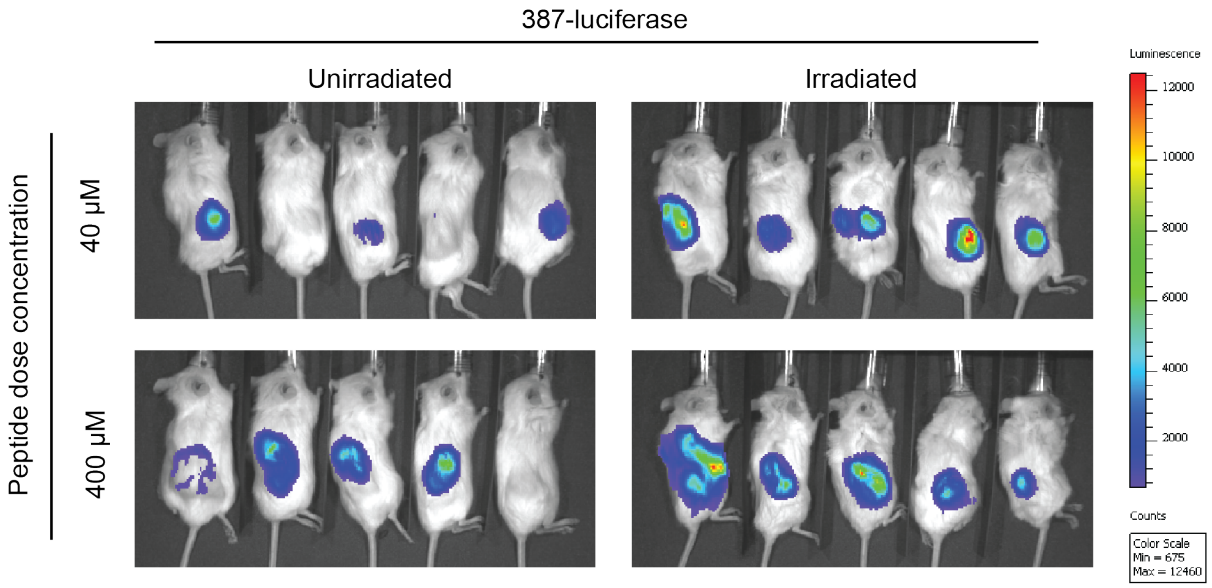

Figure S2. Luciferase assay in tumor-bearing mice. Luminescence-overlaid images of mice bearing luciferase-expressing tumors with or without irradiation (n = 5). Color bar shown on the right.

This Thesis is coauthored with Briana Prager. The thesis author was the primary author of this Thesis.

Bibliography

1. D. N. Louis, H. Ohgaki, O. D. Wiestler, W. K. Cavenee, W. K. Cavenee, P. C. Burger, A. Jouvet, B. W. Scheithauer, B. W. Scheithauer, P. Kleihues, The 2007 WHO Classification of Tumours of the Central Nervous System. *Acta Neuropathologica*, ISSN: 0001-6322 (July 6, 2007).

2. D. N. Louis, A. Perry, G. Reifenberger, A. von Deimling, A. von Deimling, D. Figarella-Branger, W. K. Cavenee, W. K. Cavenee, H. Ohgaki, O. D. Wiestler, P. Kleihues, D. W. Ellison, The 2016 World Health Organization Classification of Tumors of the Central Nervous System: A Summary. *Acta Neuropathologica*, ISSN: 0001-6322 (May 9, 2016).

3. A. Omuro, L. M. DeAngelis, Glioblastoma and Other Malignant Gliomas: A Clinical Review. *JAMA* **310**, 1842–1850, ISSN: 1538-3598, pmid: 24193082 (Nov. 6, 2013).

4. D. R. Johnson, B. P. O'Neill, Glioblastoma Survival in the United States before and during the Temozolomide Era. *J Neurooncol* **107**, 359–364, ISSN: 1573-7373 (Apr. 1, 2012).

5. R. Stupp, W. P. Mason, M. J. van den Bent, M. Weller, B. Fisher, M. J. B. Taphoorn, K. Belanger, A. A. Brandes, C. Marosi, U. Bogdahn, J. Curschmann, R. C. Janzer, S. K. Ludwin, T. Gorlia, A. Allgeier, D. Lacombe, J. G. Cairncross, E. Eisenhauer, R. O. Mirimanoff, European Organisation for Research and Treatment of Cancer Brain Tumor and Radiotherapy Groups, National Cancer Institute of Canada Clinical Trials Group, Radiotherapy plus Concomitant and Adjuvant Temozolomide for Glioblastoma. *N. Engl. J. Med.* **352**, 987–996, ISSN: 1533-4406, pmid: 15758009 (Mar. 10, 2005).

6. A. Bhaduri, E. D. Lullo, D. Jung, S. Müller, E. E. Crouch, C. S. Espinosa, T. Ozawa, B. Alvarado, J. Spatazza, C. R. Cadwell, G. Wilkins, D. Velmeshev, S. J. Liu, M. Malatesta, M. G. Andrews, M. A. Mostajo-Radji, E. J. Huang, T. J. Nowakowski, D. A. Lim, A. Diaz, D. R. Raleigh, A. R. Kriegstein, Outer Radial Glia-like Cancer Stem Cells Contribute to Heterogeneity of Glioblastoma. *Cell Stem Cell* **26**, 48–63.e6, ISSN: 1934-5909, 1875-9777, pmid: 31901251 (Jan. 2, 2020).

7. L. Cheng, Q. Wu, O. A. Guryanova, Z. Huang, Q. Huang, J. N. Rich, S. Bao, Elevated Invasive Potential of Glioblastoma Stem Cells. *Biochem Biophys Res Commun* **406**, 643–648, ISSN: 1090-2104, pmid: 21371437 (Mar. 25, 2011).

8. A. T. Parsa, J. S. Waldron, A. Panner, C. A. Crane, I. F. Parney, J. J. Barry, K. E. Cachola, J. C. Murray, T. Tihan, M. C. Jensen, D. Stokoe, R. O. Pieper, Loss of Tumor Suppressor PTEN

Function Increases B7-H1 Expression and Immunoresistance in Glioma. *Nature Medicine*, ISSN: 1078-8956 (Jan. 1, 2007).

9. F. Ricklefs, Q. Alayo, H. Krenzlin, A. B. Mahmoud, M. C. Speranza, H. Nakashima, J. Hayes, K. Lee, L. Balaj, C. Passaro, S. E. Lawler, E. A. Chiocca, Immune Evasion Mediated by PD-L1 on Glioblastoma-Derived Extracellular Vesicles. *Science Advances*, ISSN: 2375-2548 (Mar. 1, 2018).

10. K. V. Lu, J. P. Chang, C. A. Parachoniak, M. M. Pandika, M. K. Aghi, D. Meyronet, N. Isachenko, N. Isachenko, S. D. Fouse, J. J. Phillips, D. A. Cheresh, M. Park, M. Park, G. Bergers, VEGF Inhibits Tumor Cell Invasion and Mesenchymal Transition through a MET/VEGFR2 Complex. *Cancer Cell*, ISSN: 1535-6108 (July 10, 2012).

11. S. A. Mikheeva, A. M. Mikheev, A. Petit, R. P. Beyer, R. G. Oxford, L. Khorasani, J. P. Maxwell, C. A. Glackin, H. Wakimoto, I. González-Herrero, P. J. Horner, R. C. Rostomily, TWIST1 Promotes Invasion through Mesenchymal Change in Human Glioblastoma. *Molecular Cancer*, ISSN: 1476-4598 (July 20, 2010).

12. D. Sturm, H. Witt, V. Hovestadt, D. A. Khuong-Quang, D. T. W. Jones, C. Konermann, E. Pfaff, M. Tönjes, M. Sill, S. Bender, N. Jabado, S. M. Pfister, Hotspot Mutations in H3F3A and IDH1 Define Distinct Epigenetic and Biological Subgroups of Glioblastoma. *Cancer Cell*, ISSN: 1535-6108 (Oct. 16, 2012).

13. N. J. Szerlip, N. Szerlip, A. Pedraza, D. Chakravarty, M. Azim, J. J. McGuire, J. McGuire, Y. Fang, T. Ozawa, E. C. Holland, J. T. Huse, S. C. Jhanwar, T. Mikkelsen, C. Brennan, Intratumoral Heterogeneity of Receptor Tyrosine Kinases EGFR and PDGFRA Amplification in Glioblastoma Defines Subpopulations with Distinct Growth Factor Response. *Proceedings of the National Academy of Sciences of the United States of America*, ISSN: 0027-8424 (Feb. 21, 2012).

14. C. Brennan, R. G. W. Verhaak, A. McKenna, B. Campos, H. Noushmehr, S. R. Salama, S. Zheng, D. Chakravarty, J. Z. Sanborn, S. H. Berman, G. Getz, L. Chin, The Somatic Genomic Landscape of Glioblastoma. *Cell*, ISSN: 0092-8674 (Oct. 10, 2013).

15. D. W. Parsons, S. Jones, X. Zhang, J. C.-H. Lin, R. J. Leary, P. Angenendt, P. Mankoo, H. Carter, I.-M. Siu, G. L. Gallia, A. Olivi, R. McLendon, B. A. Rasheed, S. Keir, T. Nikolskaya, Y. Nikolsky, D. A. Busam, H. Tekleab, L. A. Diaz, J. Hartigan, D. R. Smith, R. L. Strausberg, S. K. N. Marie, S. M. O. Shinjo, H. Yan, G. J. Riggins, D. D. Bigner, R. Karchin, N. Papadopoulos, G. Parmigiani, B. Vogelstein, V. E. Velculescu, K. W. Kinzler, An Integrated Genomic Analysis of Human Glioblastoma Multiforme. *Science* **321**, 1807–1812, ISSN: 0036-8075, 1095-9203, pmid: 18772396 (Sept. 26, 2008).

16. A. A. Brandes, E. Franceschi, A. Tosoni, M. E. Hegi, R. Stupp, Epidermal Growth Factor Receptor Inhibitors in Neuro-Oncology: Hopes and Disappointments. *Clin Cancer Res* **14**, 957–960, ISSN: 1078-0432, 1557-3265, pmid: 18281526 (Feb. 15, 2008).

17. D. A. Reardon, P. Y. Wen, I. K. Mellinghoff, Targeted Molecular Therapies against Epidermal Growth Factor Receptor: Past Experiences and Challenges. *Neuro-Oncology* **16**, viii7–viii13, ISSN: 1522-8517 (suppl_8 Oct. 1, 2014).

18. M. F. Clarke, Clinical and Therapeutic Implications of Cancer Stem Cells. *New England Journal of Medicine* **380**, 2237–2245, ISSN: 0028-4793, pmid: 31167052 (June 6, 2019).

19. T. Reya, S. J. Morrison, M. F. Clarke, I. L. Weissman, Stem Cells, Cancer, and Cancer Stem Cells. *Nature* **414**, 105–111, ISSN: 0028-0836, pmid: 11689955 (Nov. 1, 2001).

20. J. E. Visvader, G. J. Lindeman, Cancer Stem Cells in Solid Tumours: Accumulating Evidence and Unresolved Questions. *Nature Reviews Cancer* **8**, 755–768, ISSN: 1474-1768 (10 Oct. 2008).

21. D. Bonnet, J. E. Dick, Human Acute Myeloid Leukemia Is Organized as a Hierarchy That Originates from a Primitive Hematopoietic Cell. *Nature Medicine*, ISSN: 1078-8956 (July 1, 1997).

22. C. H. Park, D. E. Bergsagel, E. A. McCulloch, Mouse Myeloma Tumor Stem Cells: A Primary Cell Culture Assay. *J Natl Cancer Inst* **46**, 411–422 (Feb. 1971).

23. S. K. Singh, I. D. Clarke, M. Terasaki, V. E. Bonn, C. Hawkins, J. Squire, P. B. Dirks, Identification of a Cancer Stem Cell in Human Brain Tumors. *Cancer Res* **63**, 5821–5828, ISSN: 0008-5472, 1538-7445, pmid: 14522905, (2020; https://cancerres.aacrjournals.org/content/63/18/5821) (Sept. 15, 2003).

24. S. K. Singh, C. Hawkins, I. D. Clarke, J. A. Squire, J. Bayani, T. Hide, R. M. Henkelman, M. D. Cusimano, P. B. Dirks, Identification of Human Brain Tumour Initiating Cells. *Nature* **432**, 396–401, ISSN: 1476-4687 (7015 Nov. 2004).

25. S. Bao, Q. Wu, S. Sathornsumetee, Y. Hao, Z. Li, A. B. Hjelmeland, Q. Shi, R. E. McLendon, D. D. Bigner, J. N. Rich, Stem Cell–like Glioma Cells Promote Tumor Angiogenesis through Vascular Endothelial Growth Factor. *Cancer Res* **66**, 7843–7848, ISSN: 0008-5472, 1538-7445, pmid: 16912155 (Aug. 15, 2006).

26. C. E. Eyler, J. N. Rich, Survival of the Fittest: Cancer Stem Cells in Therapeutic Resistance and Angiogenesis. *Journal of Clinical Oncology*, ISSN: 0732-183X (June 10, 2008).

27. Z. Li, S. Bao, Q. Wu, H. Wang, C. Eyler, S. Sathornsumetee, Q. Shi, Y. Cao, J. Lathia, R. E. McLendon, A. B. Hjelmeland, J. N. Rich, Hypoxia-Inducible Factors Regulate Tumorigenic Capacity of Glioma Stem Cells. *Cancer Cell* **15**, 501–513, ISSN: 1878-3686, pmid: 19477429 (June 2, 2009).

28. E. Binda, A. Visioli, F. Giani, N. Trivieri, O. Palumbo, S. Restelli, F. Dezi, T. Mazza, C. Fusilli, F. Legnani, M. Carella, F. D. Meco, R. Duggal, A. L. Vescovi, Wnt5a Drives an Invasive Phenotype in Human Glioblastoma Stem-like Cells. *Cancer Res* **77**, 996–1007, ISSN: 0008-5472, 1538-7445, pmid: 28011620 (Feb. 15, 2017).

29. X. Lan, D. J. Jörg, F. M. G. Cavalli, L. M. Richards, L. V. Nguyen, R. J. Vanner, P. Guilhamon, L. Lee, M. M. Kushida, D. Pellacani, N. I. Park, F. J. Coutinho, H. Whetstone, H. J. Selvadurai, C. Che, B. Luu, A. Carles, M. Moksa, N. Rastegar, R. Head, S. Dolma, P. Prinos, M. D. Cusimano, S. Das, M. Bernstein, C. H. Arrowsmith, A. J. Mungall, R. A. Moore, Y. Ma, M. Gallo, M. Lupien, T. J. Pugh, M. D. Taylor, M. Hirst, C. J. Eaves, B. D. Simons, P. B. Dirks, Fate Mapping of Human Glioblastoma Reveals an Invariant Stem Cell Hierarchy. *Nature* **549**, 227–232, ISSN: 1476-4687 (7671 Sept. 2017).

30. J. Chen, Y. Li, T.-S. Yu, R. M. McKay, D. K. Burns, S. G. Kernie, L. F. Parada, A Restricted Cell Population Propagates Glioblastoma Growth after Chemotherapy. *Nature* **488**, 522–526, ISSN: 1476-4687 (Aug. 2012).

31. B. B. Liau, C. Sievers, L. K. Donohue, S. M. Gillespie, W. A. Flavahan, T. E. Miller, A. S. Venteicher, C. H. Hebert, C. D. Carey, S. J. Rodig, S. J. Shareef, F. J. Najm, P. van Galen, H. Wakimoto, D. P. Cahill, J. N. Rich, J. C. Aster, M. L. Suvà, A. P. Patel, B. E. Bernstein, Adaptive Chromatin Remodeling Drives Glioblastoma Stem Cell Plasticity and Drug Tolerance. *Cell Stem Cell* **20**, 233–246.e7, ISSN: 1875-9777, pmid: 27989769 (Feb. 2, 2017).

32. S. Bao, Q. Wu, R. E. McLendon, Y. Hao, Q. Shi, A. B. Hjelmeland, M. W. Dewhirst, D. D. Bigner, J. N. Rich, Glioma Stem Cells Promote Radioresistance by Preferential Activation of the DNA Damage Response. *Nature* **444**, 756–760, ISSN: 1476-4687 (7120 Dec. 2006).

33. R. C. Gimple, R. L. Kidwell, L. J. Y. Kim, T. Sun, A. D. Gromovsky, Q. Wu, M. Wolf, D. Lv, S. Bhargava, L. Jiang, B. C. Prager, X. Wang, Q. Ye, Z. Zhu, G. Zhang, Z. Dong, L. Zhao, D. Lee, J. Bi, A. E. Sloan, P. S. Mischel, J. M. Brown, H. Cang, T. Huan, S. C. Mack, Q. Xie, J. N. Rich, Glioma Stem Cell–Specific Superenhancer Promotes Polyunsaturated Fatty-Acid Synthesis to Support EGFR Signaling. *Cancer Discov* **9**, 1248–1267, ISSN: 2159-8274, 2159-8290, pmid: 31201181 (Sept. 1, 2019).

34. X. Jin, L. J. Y. Kim, Q. Wu, L. C. Wallace, B. C. Prager, T. Sanvoranart, R. C. Gimple, X. Wang, S. C. Mack, T. E. Miller, P. Huang, C. L. Valentim, Q.-g. Zhou, J. S. Barnholtz-Sloan, S. Bao, A. E. Sloan, J. N. Rich, Targeting Glioma Stem Cells through Combined BMI1 and EZH2 Inhibition. *Nature Medicine* **23**, 1352–1361, ISSN: 1546-170X (11 Nov. 2017).

35. D. Dixit, B. C. Prager, R. C. Gimple, H. X. Poh, Y. Wang, Y. Wang, Q. Wu, Z. Qiu, R. L. Kidwell, L. J. Y. Kim, Q. Xie, X. Wang, J. N. Rich, The RNA m6A Reader YTHDF2 Maintains Oncogene Expression and Is a Targetable Dependency in Glioblastoma Stem Cells. *Cancer Discovery*, ISSN: 2159-8274 (Feb. 1, 2021).

36. J. Bi, T.-A. Ichu, C. Zanca, H. Yang, W. Zhang, Y. Gu, S. Chowdhry, A. Reed, S. Ikegami, K. M. Turner, W. Zhang, G. R. Villa, S. Wu, O. Quehenberger, W. H. Yong, H. I. Kornblum, J. N. Rich, T. F. Cloughesy, W. K. Cavenee, F. B. Furnari, B. F. Cravatt, P. S. Mischel, Oncogene Amplification in Growth Factor Signaling Pathways Renders Cancers Dependent on Membrane Lipid Remodeling. *Cell Metabolism* **30**, 525–538.e8, ISSN: 15504131 (Sept. 2019).

37. D. L. Schonberg, T. E. Miller, Q. Wu, W. A. Flavahan, N. K. Das, J. S. Hale, C. G. Hubert, S. C. Mack, A. M. Jarrar, R. T. Karl, A. M. Rosager, A. M. Nixon, P. J. Tesar, P. Hamerlik, B. W. Kristensen, C. Horbinski, J. R. Connor, P. L. Fox, J. D. Lathia, J. N. Rich, Preferential Iron Trafficking Characterizes Glioblastoma Stem-like Cells. *Cancer Cell* **28**, 441–455, ISSN: 1535-6108, 1878-3686, pmid: 26461092 (Oct. 12, 2015).

38. X. Wang, B. C. Prager, Q. Wu, L. J. Y. Kim, R. C. Gimple, Y. Shi, K. Yang, A. R. Morton, W. Zhou, Z. Zhu, E. A. A. Obara, T. E. Miller, A. Song, S. Lai, C. G. Hubert, X. Jin, Z. Huang, X. Fang, D. Dixit, W. Tao, K. Zhai, C. Chen, Z. Dong, G. Zhang, S. M. Dombrowski, P. Hamerlik, S. C. Mack, S. Bao, J. N. Rich, Reciprocal Signaling between Glioblastoma Stem Cells and Differentiated Tumor Cells Promotes Malignant Progression. *Cell Stem Cell* **22**, 514–528.e5, ISSN: 1934-5909 (Apr. 5, 2018).

39. W. Zhou, C. Chen, Y. Shi, Q. Wu, R. C. Gimple, X. Fang, Z. Huang, K. Zhai, S. Q. Ke, Y.-F. Ping, H. Feng, J. N. Rich, J. S. Yu, S. Bao, X.-W. Bian, Targeting Glioma Stem Cell-Derived Pericytes Disrupts the Blood-Tumor Barrier and Improves Chemotherapeutic Efficacy. *Cell Stem Cell* **21**, 591–603.e4, ISSN: 1934-5909 (Nov. 2, 2017).

40. J. Lee, S. Kotliarova, Y. Kotliarov, A. Li, Q. Su, N. M. Donin, S. Pastorino, B. W. Purow, N. Christopher, W. Zhang, J. K. Park, H. A. Fine, Tumor Stem Cells Derived from Glioblastomas Cultured in bFGF and EGF More Closely Mirror the Phenotype and Genotype of Primary Tumors than Do Serum-Cultured Cell Lines. *Cancer Cell* **9**, 391–403, ISSN: 1535-6108, 1878-3686 (May 1, 2006).

41. P. Rusu, C. Shao, A. Neuerburg, A. A. Acikgöz, Y. Wu, P. Zou, P. Phapale, T. S. Shankar, K. Döring, S. Dettling, H. Körkel-Qu, G. Bekki, B. Costa, T. Guo, O. Friesen, M. Schlotter, M. Heikenwalder, D. F. Tschaharganeh, B. Bukau, G. Kramer, P. Angel, C. Herold-Mende, B. Radlwimmer, H.-K. Liu, GPD1 Specifically Marks Dormant Glioma Stem Cells with a Distinct Metabolic Profile. *Cell Stem Cell* **25**, 241–257.e8, ISSN: 19345909 (Aug. 2019).

42. C. J. Bakkenist, M. B. Kastan, DNA Damage Activates ATM through Intermolecular Autophosphorylation and Dimer Dissociation. *Nature* **421**, 499–506, ISSN: 1476-4687 (6922 Jan. 2003).

43. M. B. Kastan, Q. Zhan, W. S. El-Deiry, T. Jacks, W. V. Walsh, B. Plunkett, B. Vogelstein, A. J. Fornace, A Mammalian Cell Cycle Checkpoint Pathway Utilizing P53 and GADD45 Is Defective in Ataxia-Telangiectasia. *Cell*, ISSN: 0092-8674 (Nov. 1, 1992).

44. P. A. Riley, Free Radicals in Biology: Oxidative Stress and the Effects of Ionizing Radiation. *International Journal of Radiation Biology*, ISSN: 0955-3002 (Jan. 1, 1994).

45. D. Trachootham, J. Alexandre, P. Huang, Targeting Cancer Cells by ROS-Mediated Mechanisms: A Radical Therapeutic Approach? *Nature Reviews Drug Discovery* **8**, 579–591, ISSN: 1474-1784 (7 July 2009).

46. M. Diehn, R. W. Cho, N. A. Lobo, T. Kalisky, M. J. Dorie, A. N. Kulp, D. Qian, J. Lam, L. Ailles, M. Wong, I. L. Weissman, M. F. Clarke, Association of Reactive Oxygen Species Levels and Radioresistance in Cancer Stem Cells. *Nature*, ISSN: 0028-0836 (Apr. 9, 2009).

47. D. Hambardzumyan, O. J. Becher, M. K. Rosenblum, P. P. Pandolfi, K. Manova-Todorova, E. C. Holland, PI3K Pathway Regulates Survival of Cancer Stem Cells Residing in the Perivascular Niche Following Radiation in Medulloblastoma in Vivo. *Genes & Development*, ISSN: 0890-9369 (Feb. 15, 2008).

48. N. K. Kurrey, S. P. Jalgaonkar, A. V. Joglekar, A. D. Ghanate, P. D. Chaskar, R. Y. Doiphode, S. A. Bapat, Snail and Slug Mediate Radioresistance and Chemoresistance by Antagonizing P53-Mediated Apoptosis and Acquiring a Stem-Like Phenotype in Ovarian Cancer Cells. *STEM CELLS* **27**, 2059–2068, ISSN: 1549-4918 (2009).

49. T. M. Phillips, W. H. McBride, F. Pajonk, The Response of CD24 /Low /CD44 + Breast Cancer–Initiating Cells to Radiation. *Journal of the National Cancer Institute*, ISSN: 0027-8874 (Dec. 20, 2006).

50. Y. Shi, O. A. Guryanova, W. Zhou, C. Liu, Z. Huang, X. Fang, X. Wang, C. Chen, Q. Wu, Z. He, W. Wang, W. Zhang, T. Jiang, Q. Liu, Y. Chen, W. Wang, J. Wu, L. Kim, R. C. Gimple, H. Feng, H.-F. Kung, J. S. Yu, J. N. Rich, Y.-F. Ping, X.-W. Bian, S. Bao, Ibrutinib Inactivates BMX-STAT3 in Glioma Stem Cells to Impair Malignant Growth and Radioresistance. *Science Translational Medicine* **10**, ISSN: 1946-6234, 1946-6242, pmid: 29848664 (May 30, 2018).

51. J. Wang, T. P. Wakeman, J. D. Lathia, A. B. Hjelmeland, X.-F. Wang, R. R. White, J. N. Rich, B. A. Sullenger, Notch Promotes Radioresistance of Glioma Stem Cells. *Stem Cells*, ISSN: 1066-5099 (Nov. 17, 2009).

52. M. Baumann, M. Krause, R. Hill, Exploring the Role of Cancer Stem Cells in Radioresistance. *Nature Reviews Cancer* **8**, 545–554, ISSN: 1474-1768 (7 July 2008).

53. J. W. Kehoe, B. K. Kay, Filamentous Phage Display in the New Millennium. *Chem. Rev.* **105**, 4056–4072, ISSN: 0009-2665 (Nov. 1, 2005).

54. G. P. Smith, Filamentous Fusion Phage: Novel Expression Vectors That Display Cloned Antigens on the Virion Surface. *Science*, ISSN: 0036-8075 (June 14, 1985).

55. C. F. Barbas, A. S. Kang, R. A. Lerner, S. J. Benkovic, Assembly of Combinatorial Antibody Libraries on Phage Surfaces: The Gene III Site. *Proceedings of the National Academy of Sciences of the United States of America*, ISSN: 0027-8424 (Sept. 15, 1991).

56. J. J. Devlin, L. C. Panganiban, P. E. Devlin, Random Peptide Libraries: A Source of Specific Protein Binding Molecules. *Science*, ISSN: 0036-8075 (July 27, 1990).

57. D. M. Brown, E. Ruoslahti, Metadherin, a Cell Surface Protein in Breast Tumors That Mediates Lung Metastasis. *Cancer Cell* **5**, 365–374, ISSN: 1535-6108 (Apr. 1, 2004).

58. J. Kim, C. She, M. Potez, P. Huang, Q. Wu, B. C. Prager, Z. Qiu, S. Bao, J. N. Rich, J. K. C. Liu, Phage Display Targeting Identifies EYA1 as a Regulator of Glioblastoma Stem Cell Maintenance and Proliferation. *Stem Cells*, ISSN: 1549-4918, pmid: 33594762 (Feb. 16, 2021).

59. P. Laakkonen, K. Porkka, J. A. Hoffman, E. Ruoslahti, A Tumor-Homing Peptide with a Targeting Specificity Related to Lymphatic Vessels. *Nat Med* **8**, 751–755, ISSN: 1546-170X (7 July 2002).

60. J. K. Scott, G. P. Smith, Searching for Peptide Ligands with an Epitope Library. *Science*, ISSN: 0036-8075 (July 27, 1990).

61. S. L. Hart, A. M. Knight, R. P. Harbottle, A. Mistry, H. D. Hunger, D. F. Cutler, R. Williamson, C. Coutelle, Cell Binding and Internalization by Filamentous Phage Displaying a Cyclic Arg-Gly-Asp-Containing Peptide. *Journal of Biological Chemistry* **269**, 12468–12474, ISSN: 0021-9258, 1083-351X, pmid: 8175653 (Apr. 29, 1994).

62. K. A. Kelly, J. R. Allport, A. Tsourkas, V. R. Shinde-Patil, L. Josephson, R. Weissleder, Detection of Vascular Adhesion Molecule-1 Expression Using a Novel Multimodal Nanoparticle. *Circulation Research*, ISSN: 0009-7330 (Feb. 18, 2005).

63. Z. Li, R. Zhao, X. Wu, Y. Sun, M. Yao, J. Li, Y. Xu, J. Gu, Identification and Characterization of a Novel Peptide Ligand of Epidermal Growth Factor Receptor for Targeted Delivery of Therapeutics. *The FASEB Journal*, ISSN: 0892-6638 (Dec. 1, 2005).

64. M. Nahrendorf, F. A. Jaffer, K. A. Kelly, D. E. Sosnovik, E. Aikawa, P. Libby, R. Weissleder, Noninvasive Vascular Cell Adhesion Molecule-1 Imaging Identifies Inflammatory Activation of Cells in Atherosclerosis. *Circulation*, ISSN: 0009-7322 (Oct. 3, 2006).

65. W. Arap, W. Arap, R. Pasqualini, E. Ruoslahti, Cancer Treatment by Targeted Drug Delivery to Tumor Vasculature in a Mouse Model. *Science*, ISSN: 0036-8075 (Jan. 16, 1998).

66. J. K. Liu, D. Lubelski, D. L. Schonberg, Q. Wu, J. S. Hale, W. A. Flavahan, E. E. Mulkearns-Hubert, J. Man, A. B. Hjelmeland, J. Yu, J. D. Lathia, J. N. Rich, Phage Display Discovery of Novel Molecular Targets in Glioblastoma-Initiating Cells. *Cell Death & Differentiation* **21**, 1325–1339, ISSN: 1476-5403 (8 Aug. 2014).

67. A. P. Mann, P. Scodeller, S. Hussain, J. Joo, E. Kwon, G. B. Braun, T. Mölder, Z.-G. She, V. R. Kotamraju, B. Ranscht, S. Krajewski, T. Teesalu, S. Bhatia, M. J. Sailor, E. Ruoslahti, A Peptide for Targeted, Systemic Delivery of Imaging and Therapeutic Compounds into Acute Brain Injuries. *Nature Communications* **7**, 11980, ISSN: 2041-1723 (1 June 28, 2016).

68. *What Is Ph.D.™ Phage Display? — NEB* (2021; https://www.neb.com/faqs/0001/01/01/whatisphdphagedisplay).

69. M. Jackson, F. Hassiotou, A. Nowak, Glioblastoma Stem-like Cells: At the Root of Tumor Recurrence and a Therapeutic Target. *Carcinogenesis* **36**, 177–185, ISSN: 0143-3334 (Feb. 1, 2015).

70. A. Bretscher, K. Edwards, R. G. Fehon, ERM Proteins and Merlin: Integrators at the Cell Cortex. *Nature Reviews Molecular Cell Biology* **3**, 586–599, ISSN: 1471-0080 (8 Aug. 2002).

71. A. Naba, C. Reverdy, D. Louvard, M. Arpin, Spatial Recruitment and Activation of the Fes Kinase by Ezrin Promotes HGF-Induced Cell Scattering. *The EMBO Journal* **27**, 38–50, ISSN: 0261-4189 (Jan. 9, 2008).

72. D.-C. Kang, Z.-Z. Su, D. Sarkar, L. Emdad, D. J. Volsky, P. B. Fisher, Cloning and Characterization of HIV-1-Inducible Astrocyte Elevated Gene-1, AEG-1. *Gene* **353**, 8–15, ISSN: 0378-1119, pmid: 15927426 (June 20, 2005).

73. H. J. Thirkettle, I. G. Mills, H. C. Whitaker, D. E. Neal, Nuclear LYRIC/AEG-1 Interacts with PLZF and Relieves PLZF-Mediated Repression. *Oncogene* **28**, 3663–3670, ISSN: 1476-5594 (41 Oct. 2009).

74. D. Sarkar, E. S. Park, L. Emdad, S.-G. Lee, Z.-z. Su, P. B. Fisher, Molecular Basis of Nuclear Factor-B Activation by Astrocyte Elevated Gene-1. *Cancer Res* **68**, 1478–1484 (Mar. 1, 2008).

75. T. R. Pearce, K. Shroff, E. Kokkoli, Peptide Targeted Lipid Nanoparticles for Anticancer Drug Delivery. *Advanced Materials* **24**, 3803–3822, ISSN: 1521-4095 (2012).

76. K. N. Sugahara, T. Teesalu, P. P. Karmali, V. R. Kotamraju, L. Agemy, O. M. Girard, D. Hanahan, R. F. Mattrey, E. Ruoslahti, Tissue-Penetrating Delivery of Compounds and Nanoparticles into Tumors. *Cancer Cell* **16**, 510–520, ISSN: 1535-6108, 1878-3686, pmid: 19962669 (Dec. 8, 2009).

77. Q. Hu, X. Gao, G. Gu, T. Kang, Y. Tu, Z. Liu, Q. Song, L. Yao, Z. Pang, X. Jiang, H. Chen, J. Chen, Glioma Therapy Using Tumor Homing and Penetrating Peptide-Functionalized PEG-PLA Nanoparticles Loaded with Paclitaxel. *Biomaterials* **34**, 5640–5650, ISSN: 1878-5905, pmid: 23639530 (July 2013).

78. M. M. Patel, B. R. Goyal, S. V. Bhadada, J. S. Bhatt, A. F. Amin, Getting into the Brain. *CNS Drugs* **23**, 35–58, ISSN: 1179-1934 (Jan. 1, 2009).

79. B. D. Choi, M. V. Maus, C. H. June, J. H. Sampson, Immunotherapy for Glioblastoma: Adoptive T-Cell Strategies. *Clin Cancer Res* **25**, 2042–2048 (Apr. 1, 2019).

80. M. Lim, Y. Xia, C. Bettegowda, M. Weller, Current State of Immunotherapy for Glioblastoma. *Nature Reviews Clinical Oncology* **15**, 422–442, ISSN: 1759-4782 (7 July 2018).

81. City of Hope Medical Center, "A Phase 1 Cellular Immunotherapy Study of Intraventricularly Administered Autologous HER2-Targeted Chimeric Antigen Receptor (HER2-CAR) T Cells in Patients With Brain and/or Leptomeningeal Metastases From HER2 Positive Cancers", Clinical trial registration NCT03696030 (clinicaltrials.gov, Aug. 28, 2020), (2021; https://clinicaltrials.gov/ct2/show/NCT03696030).

82. City of Hope Medical Center, "Phase I Study of Cellular Immunotherapy Using Memory-Enriched T Cells Lentivirally Transduced to Express a HER2-Specific, Hinge-Optimized,

41BB-Costimulatory Chimeric Receptor and a Truncated CD19 for Patients With Recurrent/Refractory Malignant Glioma", Clinical trial registration NCT03389230 (clinicaltrials.gov, Dec. 7, 2020), (2021; https://clinicaltrials.gov/ct2/show/NCT03389230).

83. City of Hope Medical Center, "Phase I Study of Cellular ImmunoTx Using Memory Enriched T Cells Lentivirally Transduced to Express an IL13R2-Specific, Hinge-Optimized, 41BB-Costimulatory Chimeric Receptor and a Truncated CD19 for Pts With Rec/Ref MaligGlioma", Clinical trial registration NCT02208362 (clinicaltrials.gov, Feb. 9, 2021), (2021; https://clinicaltrials.gov/ct2/show/NCT02208362).

84. A. Spandidos, X. Wang, H. Wang, B. Seed, PrimerBank: A Resource of Human and Mouse PCR Primer Pairs for Gene Expression Detection and Quantification. *Nucleic Acids Research* **38**, D792–D799, ISSN: 0305-1048 (suppl_1 Jan. 1, 2010).

85. X. Wang, B. Seed, A PCR Primer Bank for Quantitative Gene Expression Analysis. *Nucleic Acids Research* **31**, e154–e154, ISSN: 0305-1048 (Dec. 15, 2003).

86. N. E. Sanjana, O. Shalem, F. Zhang, Improved Vectors and Genome-Wide Libraries for CRISPR Screening. *Nature Methods* **11**, 783–784, ISSN: 1548-7105 (8 Aug. 2014).

87. O. Shalem, N. E. Sanjana, E. Hartenian, X. Shi, D. A. Scott, T. S. Mikkelsen, D. Heckl, B. L. Ebert, D. E. Root, J. G. Doench, F. Zhang, Genome-Scale CRISPR-Cas9 Knockout Screening in Human Cells. *Science* **343**, 84–87, ISSN: 0036-8075, 1095-9203, pmid: 24336571 (Jan. 3, 2014).

88. J. G. Doench, N. Fusi, M. Sullender, M. Hegde, E. W. Vaimberg, K. F. Donovan, I. Smith, Z. Tothova, C. Wilen, R. Orchard, H. W. Virgin, J. Listgarten, D. E. Root, Optimized sgRNA Design to Maximize Activity and Minimize Off-Target Effects of CRISPR-Cas9. *Nature Biotechnology* **34**, 184–191, ISSN: 1546-1696 (2 Feb. 2016).

89. K. R. Sanson, R. E. Hanna, M. Hegde, K. F. Donovan, C. Strand, M. E. Sullender, E. W. Vaimberg, A. Goodale, D. E. Root, F. Piccioni, J. G. Doench, Optimized Libraries for CRISPR-Cas9 Genetic Screens with Multiple Modalities. *Nature Communications* **9**, 5416, ISSN: 2041-1723 (1 Dec. 21, 2018).